Journal of Hydrology 625 (2023) 130122

Contents lists available at ScienceDirect

Journal of Hydrology

journal homepage: www.elsevier.com/locate/jhydrol

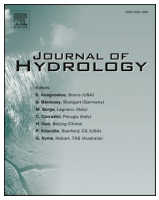

Research papers

Expressive fluxes over Amazon floodplain revealed by 2D hydrodynamic modelling

Alice César Fassoni-Andrade [a,b,c,*], Rodrigo Cauduro Dias de Paiva [a], Sly Wongchuig [d], Cláudio Barbosa [e], Fabien Durand [b,d], Thiago Sanna Freire Silva [c]

[a] Institute of Hydraulic Research, Federal University of Rio Grande do Sul (UFRGS), Porto Alegre 91501-970, Brazil
[b] Laboratório de Geoquímica, Instituto de Geociencias, Universidade de Brasilia, Brasilia 70.910-900, Brazil
[c] Biological and Environmental Sciences, Faculty of Natural Sciences, University of Stirling, Stirling FK9 4LA, UK
[d] Laboratoire d'Etudes en Géophysique et Océanographie Spatiales (LEGOS), Université Toulouse, IRD, CNRS, CNES, UPS, Toulouse, France
[e] Instrumentation Lab for Aquatic Systems (LabISA), Earth Observation Coordination of National Institute for Space Research (INPE), São José dos Campos, SP, Brazil

A B S T R A C T

Water fluxes in the Amazon River floodplain affect hydrodynamic and ecological processes from local to global scales, but they remain poorly understood due to difficult accessibility and limited data. We characterized the hydrodynamics of eight floodplain units of the central Amazon River (40000 km^2) using the 2D hydraulic model HEC-RAS. High resolution modelling (~400 m) improved the representation of river and floodplain discharge, water surface elevation (77 cm accuracy) and flood extent (~80% - high water period, ~52% - low water period) compared to past modelling studies. Our results show that floodplain flows during floods are very intense with upstream inflow and downstream outflow of the floodplain units. These gross flows are much larger than the net flows, with values of up to 20% of the Amazon River discharge and residence time around 6 days during floods (several months during low water period). Water extent did not show strong interannual variability during floods as the volume stored in the floodplain did, possibly due to topographic constraints. Significant hysteresis in flood extent and volume, and active and storage zones on the floodplain highlight the complexity of floodplain hydrodynamics. Extreme floods strongly impacted the onset and duration of the flood by up to one month and, consequently on duration of high water renewal period with the river. Our characterization is important to assess the effects of extreme floods on riverine communities, understand nutrient and sediment variations in the floodplain, and characterize the export of water, sediment, and carbon flux to the ocean from the world's largest hydrological system.

1. Introduction

The Amazon is the largest river system in the world in both drainage area and discharge. Its annual flood pulse seasonality thus causes large annual variation in water surface elevation and flooded area in Amazonian floodplains. Water level amplitude can reach up to 13 m (Birkett et al., 2002) and the entire water surface extent of the basin varies between 284200 km^2 during lowest water levels (October-November) and 633500 km^2 during highest levels (April-May) (Fleischmann et al., 2022; Hess et al., 2015). Moreover, vertically averaged bidirectional flows and water residence times in Amazonian floodplains are dynamic in space and time, producing complex patterns of water surface elevation variation (Alsdorf et al., 2007; Cao et al., 2018). The lower Amazon River is also unique in that the largest flux of fluvial water in the world passes through the reach (average discharge of ~ 190000 m^3 s^{-1}), more than four times larger than the second largest basin in the world (average discharge of Congo River ~ 40000 m^3 s^{-1}; Alsdorf et al., 2016). The Amazon River flood pulse also has strong influence on regional and global processes such as sediment transport (Armijos et al., 2020; Dunne et al., 1998), geomorphic evolution (Fricke et al., 2019; Latrubesse and Franzinelli, 2002), vegetation distribution (Ferreira-Ferreira et al., 2014), seed dispersal (Melack et al., 2009), carbon dioxide (Abril et al., 2014) and methane emissions (Basso et al., 2021), and commercial and subsistence fisheries (Duponchelle et al., 2021). Therefore, understanding the water flow between the Amazon River and its associated floodplain is of great importance for better understanding all these processes.

The floodplains along the Amazon River mainstem vary between 20 and 50 km wide over the 1100 km reach between the confluence of the Negro and Xingu rivers. Given its sheer extent and difficult access, the existence of reliable, continuous and spatially representative in situ measurements of topography, water level, and water flow are limited making the detailed hydrodynamics of the Amazon river-floodplain system still poorly known. Low resolution hydrologic and hydrodynamic models have been used to understand large-scale hydrodynamics processes and the role of floodplains in the Amazon basin (Beighley

* Corresponding author.
E-mail addresses: alice.fassoni@unb.br, alice.fassoni@gmail.com (A. César Fassoni-Andrade).

https://doi.org/10.1016/j.jhydrol.2023.130122
Received 24 March 2023; Received in revised form 4 August 2023; Accepted 17 August 2023
Available online 9 September 2023

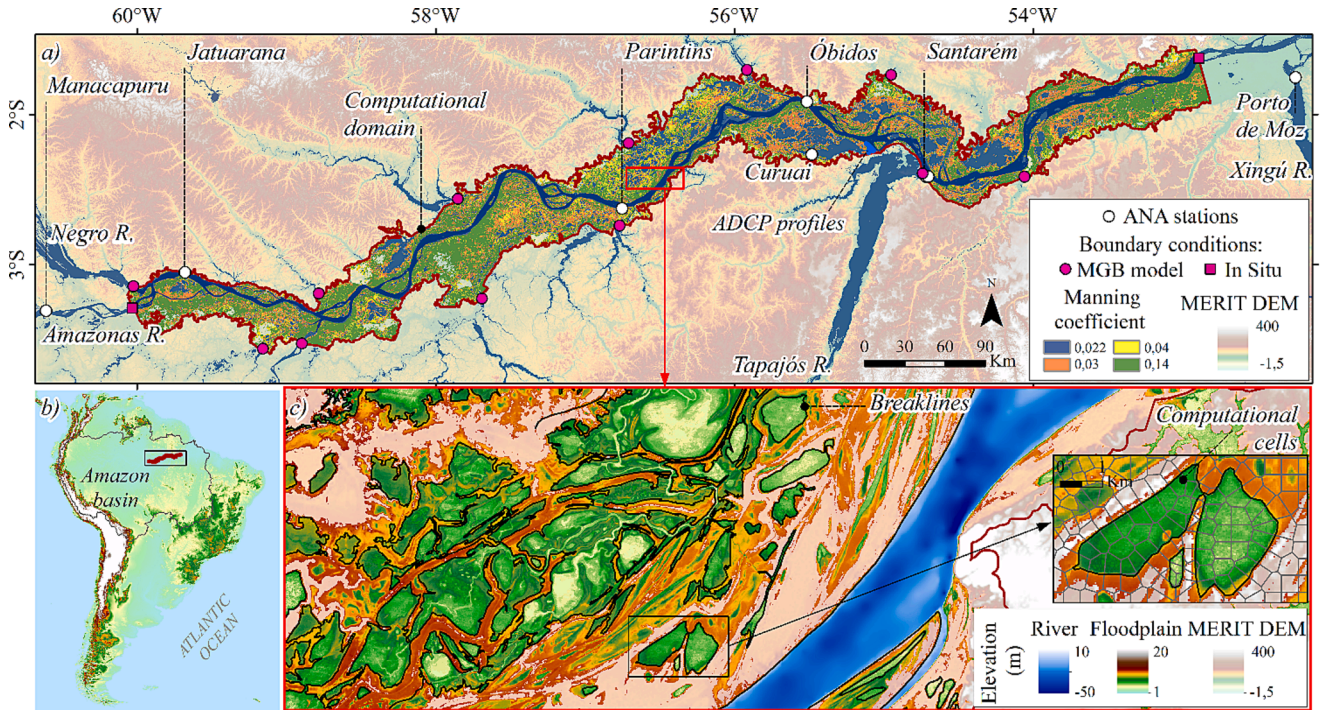

Fig. 1. a) Location of computational domain (~40000 km^2), boundary conditions and ANA stations. Manning coefficient mapping (within boundary) and topographic model MERIT DEM (outside boundary). b) Location of the central region of the Amazon basin. c) Detail of the floodplain topography, position of computational cells and breaklines used in the model.

et al., 2009; Coe et al., 2008; Correa et al., 2017; Getirana et al., 2012; Luo et al., 2017; de Paiva et al. 2013; Sorribas et al., 2020; Yamazaki et al., 2011). These studies have shown that water exchange between river and floodplain has the same order of magnitude as river discharge (c.a. 10^4 to 10^5 m^3s^{-1}; Sorribas et al., 2020) and can represent between 3% and 40% of the river discharge depending on seasonal period (Getirana et al., 2012; Richey et al., 1989; Sorribas et al., 2020; Wilson et al., 2007). Water stored in floodplains can have a residence time of more than 300 days (Sorribas et al., 2020) and thus plays an important role in delaying and attenuating the flood pulse wave (Getirana et al., 2012; de Paiva et al. 2013; Yamazaki et al., 2011). Still, while these models adequately represent river hydraulics (e.g., full Saint-Venant equation, particle-tracking model), they are simplified to represent floodplain hydrodynamics such as bidirectional flows and it is not possible to characterize the hydrodynamic processes in detail, which can be better represented with two-dimensional numerical models.

Regional applications of two-dimensional hydraulic models have allowed better representation of floodplain hydrodynamics. Wilson et al. (2007) evaluated the water exchange between the Amazon River and the adjacent floodplain over a 240 km-long reach, but floodplain drainage processes in this model were poorly represented due to errors in the topographic data. Yamazaki et al. (2012a) and Baugh et al. (2013) have improved the accuracy of this simulation by correcting topographic errors, but these studies used the SRTM3 digital elevation model (DEM) in open water areas, where the lakes are represented by a flat surface. Global elevation models do not capture the complex topography of the central Amazon floodplain, composed of many interconnected lakes and channels (Trigg et al., 2012) and vegetation types (Hess et al., 2015). In addition, Baugh et al. (2013), de Paiva et al. (2013), Yamazaki et al. (2012a) and Getirana et al. (2012) have shown that topography is the main source of current uncertainty in modeling Amazon river-floodplain system water flows.

Only a handful of lakes in the Amazon floodplain have in situ bathymetry data available: Lago Calado (73 km^2; Lesack & Melack, 1995), Lago Grande de Curuai (2440 km^2; Barbosa et al., 2006) and Lago Janauacá (786 km^2; Pinel et al., 2015). The availability of high resolution topography has allowed implementation of local, two-dimensional models that have provided important contributions to understanding the hydrology of river-floodplain systems (Bonnet et al., 2017, 2008; Ji et al., 2019; Lesack and Melack, 1995; Pinel et al., 2019; Rudorff et al., 2014a, 2014b). Floodplain water residence times estimated by these local models range from 19 to 74 days (Bonnet et al., 2017; Rudorff et al., 2014a). In Lake Calado, local runoff represented the dominant source of water input with 57% (Lesack and Melack, 1995), and maximum river water volume in the lake is observed before the river flood due to local contributions (Ji et al., 2019). Conversely, the main water input for Lago Grande de Curuai and Lago Janauacá was river, representing, respectively 77% (Bonnet et al., 2008) and 93% (Bonnet et al., 2017) of all sources. Rudorff et al. (2014b) showed that overbank flow in the Curuai floodplain accounts for 93% of the total flow in the river-floodplain direction and 54% of the flow in the opposite direction (floodplain-river), with the remaining flow being channelized. These lakes illustrate the remarkable heterogeneity of river-floodplain hydrodynamics in Amazon floodplain systems. Since water fluxes in these systems are also not described in most studies - the first (and only, to our knowledge) validation of water velocity in an Amazonian floodplain has been performed by Pinel et al. (2019) for Lake Janauacá - there are still significant knowledge gaps about the hydrology and hydrodynamics of the complex and globally important Amazon river-floodplain system.

Aiming at filling this gap, Fassoni-Andrade et al. (2020a) have reconstructed the topography of a large reach of the Amazon River floodplain (~40000 km^2) at 30 m spatial resolution using remote sensing data. This dataset thus presents a unique opportunity to investigate bidirectional flows and river-floodplain water exchanges over a large floodplain with better topographic representation than provided by global DEMs, using a two-dimensional hydraulic model.

To date, we are not aware of any study that has tested and applied comprehensive and detailed 2D hydrodynamic modeling over large floodplains in the Amazon. Such an assessment could address questions not yet fully explored, such as (1) What is the spatial distribution of hydrodynamic processes across the Amazon River and floodplain landscape? (2) What is the space–time variation of flows, velocity, storage

volume, depth, flood extent, and residence time in the floodplain? (3) How do bidirectional water flows vary in the floodplain? (4) How much water flows through the floodplain? (5) What is the impact of large and small floods on the hydrodynamic variables? (6) How can state-of-the-art hydrodynamic models contribute to describe these hydrodynamic processes?

Thus, the goal of this study is to provide a comprehensive and detailed characterization of the Amazon River and floodplain hydrodynamics by means of the first detailed 2D hydrodynamic model of this region using unprecedented topography data (Fassoni-Andrade et al., 2020a). The study is divided into methodology (Section 2), validation (Section 3), results (Section 4), and conclusions (Section 5). In sections 3 and 4 we synthesize the main results in key messages about the modeling and the hydrodynamics processes, what we call learned lessons.

2. Data sets and methods

2.1. Hydraulic model and simulation domain

The HEC-RAS model allows the representation of two-dimensional flows from the numerical solution of the shallow water equations. It represents the inertia terms, pressure gradient and gravitational effects, friction, turbulence, and Coriolis effects. Details of the formulations and numerical schemes used in the model (6.1.0 version) can be found in Brunner (2016).

The model was applied to a 1100 km reach of the Amazon River between the confluence of the Negro and Xingu rivers, where an extensive floodplain is present (Fig. 1). The computational domain, which covers ~ 40000 km^2, was delimited from a 1 km buffer of the Amazon wetlands mask (Hess et al., 2015; Fig. 1). The simulation covered 3 hydrological years (November 2007 to October 2010) comprising normal (mid-2008), large (mid-2009) and small (mid-2010) flood magnitudes (Filizola et al., 2014), i.e. the condition of the flood in relation to the discharge. A period of 5 months before November 2007 was considered as model initialization, allowing the filling of the floodplain before the evaluated period.

The time series of Amazon discharge from the Manacapuru station, located ~ 67 km upstream of the domain upstream limit (Fig. 1) was used as the upstream inlet boundary condition for the Amazon River. Detailed information for this and other stations operated by the Agência Nacional de Águas e Saneamento Básico (ANA, Brazilian water agency; snirh.gov.br/hidroweb/serieshistoricas) are shown in Table A1 (Appendix). The water level time series from the Porto de Moz station (operated by ANA) was used as boundary condition downstream, representing the water level of the Xingu River at its confluence with the Amazon River, ~77 km downstream from the model domain (Fig. 1). Due to the backwater effect on the Amazon River tributaries (Meade et al., 1991), the station can be considered representative of the Amazon River level. The vertical levelling of this station (EGM 2008) was done considering a virtual station from Sentinel-3A satellite close to the boundary condition (station amz_amz_s3a_0433_01; hydroweb.theia-land.fr/) with an estimated bias of 1.108 m (49 records between 2016 and 2020). Tidal effect from water level was filtered using a moving window of 28 days (Pugh and Woodworth, 2014).

The discharges of the main tributaries in the model domain were considered as boundary conditions from simulated data performed by Siqueira et al. (2018) using the MGB hydrological model (Collischonn et al., 2007). For this, 12 tributaries (Fig. 1) were selected as they represent up to 99% of the average modeled flow contributing to the computational domain, calculated from the MGB model of Siqueira et al. (2018).

2.2. Topography and computational mesh

A composite topography map was produced by merging several databases. In the Amazon River and open water areas of the floodplain, the topography estimated by Fassoni-Andrade et al. (2020a) at 30 m spatial resolution was used (Fig. 1a; available at data.mendeley.com/datasets/vn599y9szb/1). This mapping was created by digitizing nautical charts for the rivers, and using the Flood2Topo method (Fassoni-Andrade et al., 2020b) via optical satellite data. The DEM represents the topographic variation of lakes and narrow channels (greater than 30 m) in the open water regions of the floodplain such that the drainage of these areas can be represented in the model. Validation using locally derived bathymetry showed a root mean square error (RMSE) of 90 cm for the floodplain bottom level. However, the bathymetry of deeper, always-flooded regions in the floodplain was underestimated as it represents the lowest observed water level in 30 years. The average bias of the river bathymetry was documented as 5 m (Fassoni-Andrade et al., 2020a) and discounted in the elevation values.

In flooded vegetation and upland areas, topography was obtained from the MERIT DEM v1.0.1 (Multi-Error-Removed Improved-Terrain DEM; available at hydro.iis.u-tokyo.ac.jp/~yamadai/MERIT_DEM/). We chose this model due to its global coverage and removal of absolute bias, noise, and vegetation height from SRTM3 DEM and AW3D-30 m v1 data (Yamazaki et al., 2017). The vertical reference of the model (EGM 1996) was adjusted to the EGM 2008 model using the MSP program GEOTRANS 3.7 (available at: earth-info.nga.mil/GandG/geotrans/index.html#zza1).

The HEC-RAS model uses an unstructured computational mesh in which the orientation and size of the cells can vary according to topography, so that breaklines can be included to define the orientation of the computational cell faces. We added breaklines (e.g., Fig. 1d) considering a manual digitization of the topographic contours of the river banks. In floodplain areas we used the isolines formed by the 90% and 60% flood frequency thresholds of the flood frequency map elaborated by Fassoni-Andrade et al. (2020a). These thresholds (90% and 60%) roughly delineate the location of greater topographic variations, such as riverbanks. The computational mesh was generated with a nominal cell size of 400 m (detailed representation through breaklines in smaller features) and resulted in ~ 260000 cells. Despite the nominal size of 400 m, smaller features were represented through the breaklines considering the 30 m topography.

2.3. Manning's roughness coefficient

Manning's roughness coefficient value in the Amazon River was calibrated for the period from September 1, 2006, to August 31, 2007 (1 year). From trial and error values ranging from 0.02 to 0.03, a Manning coefficient of 0.022 resulted yielded the lowest RMSE between simulated and observed water levels at the ANA gauging stations at Jatuarana (0.19 m), Parintins (0.13 m), and Santarém (0.21 m) (Fig. 1). For reference, Lefavour and Alsdorf (2005) assumed a Manning coefficient of 0.025 with an error of 12% for discharge estimation in the Solimões River. Wilson et al., (2007) calibrated a regional hydraulic model of the lower Solimões River using values in the range between 0.022 and 0.028 based on the estimation of Lefavour and Alsdorf (2005). The value we found is low compared to values from Rudorff et al. (2014a; 0.031) and Trigg et al. (2009; 0.032) for the Amazon River, but it is within the uncertainty bound considered by Lefavour and Alsdorf (2005) of 0.025 ± 0.003.

Manning coefficient map in the floodplain (Fig. 1) was prepared based on the Amazon wetland land cover mapping of Hess et al. (2015) and values were assigned for each class based on recommendations by Arcement and Schneider (1989) and Chow (1959), according to Table A2 (Appendix). The model uncertainty caused by this parameter was assessed by means of two additional model runs where Manning coefficient values were perturbed by ± 30%, according to Chow's table for the same vegetation cover (Chow, 1959).

Table 1
Fit metric for HESS and ALOS products considering the low and high water periods.

	Low water (November) Flooded area	*F* 2007	*F*	*F*2009	High water (May) Flooded area	*F* 2008	*F*2009	*F*2010
HESS	17942 km^2	52%	52%	52%	31278 km^2	81%	82%	81%
ALOS 2014–2015	8939 km^2	51%	50%	48%	21760 km^2	58%	59%	58%
ALOS 2015–2016	8130 km^2	46%	45%	44%	20130 km^2	56%	56%	56%
ALOS 2016–2017	8641 km^2	49%	48%	47%	20679 km^2	56%	56%	56%

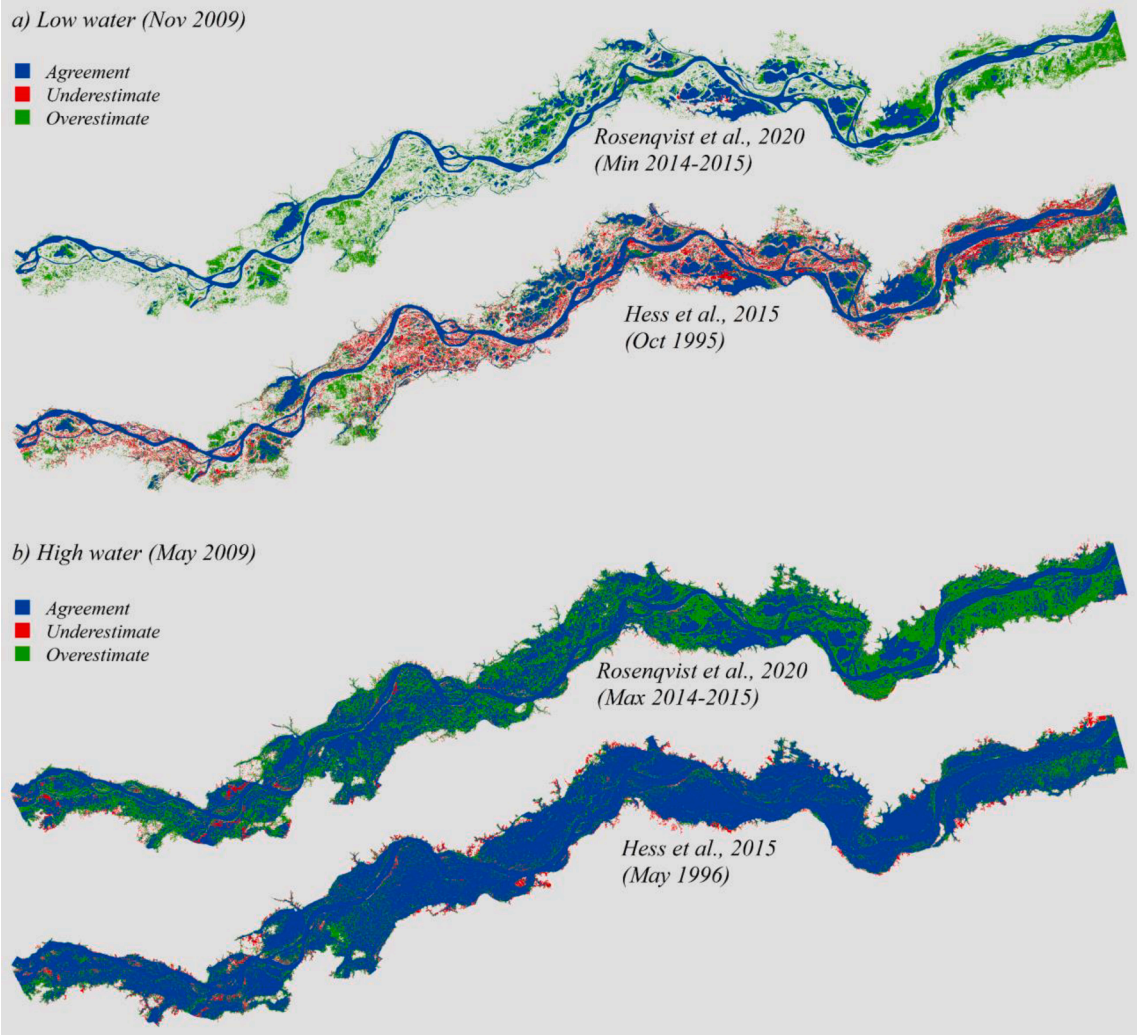

Fig. 2. Flood extent mapped by the model and remote sensing products (blue), flood extent not mapped by the model (underestimate), and flood extent mapped only by the model (overestimate) considering ALOS and HESS products and simulated in November, the 1st (a) and May, the 1st (b) of 2009. (For interpretation of the references to colour in this figure legend, the reader is referred to the web version of this article.)

2.4. Metrics of model performance

The hydrodynamic model was validated against in situ and satellite observations to assess its capability to represent flooded area, water surface elevation and water flow in both river and floodplain. Several remote sensing-derived Amazon flood extent databases have been developed in recent years to characterize flooding in Amazon (Fassoni-Andrade et al., 2021). As this is far from a trivial mapping task, these different approaches have led to remarkable disagreements, as shown by the comparison documented in Fleischmann et al. (2022). We used here two basin-scale databases that considered periods of maximum and minimum inundation (Hess et al., 2015; Rosenqvist et al., 2020). The map by Hess et al. (2015) (hereafter called HESS) is the most widely used dataset for validating hydrologic-hydrodynamic models in the Amazon basin, and it depicts wetland inundation and vegetation classes for the central Amazon basin based on JERS-1 synthetic aperture radar (SAR) images acquired during Oct.-Nov. 1995 and May-July 1996 with a spatial resolution of 100 m (available at https://daac.ornl.gov/LBA/guides/LC07_Amazon_Wetlands.html). Rosenqvist's mapping (hereafter called ALOS) (Rosenqvist et al., 2020) conversely considers

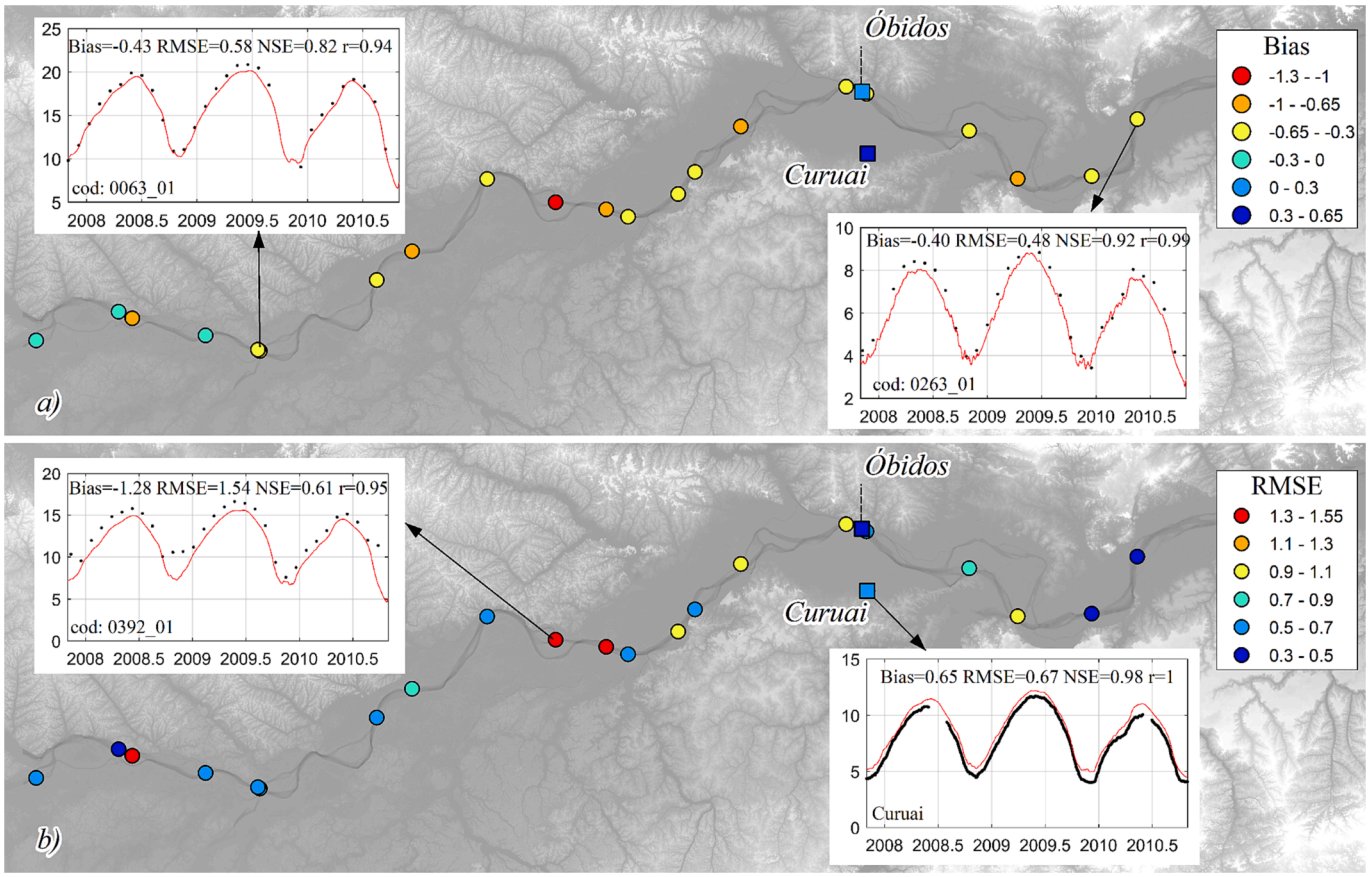

Fig. 3. Validation of absolute water surface elevation derived from the model against in-situ observations of gauging stations (squares) and satellite altimetry data (circles). Spatial distribution of model performance statistics: Bias (a) and RMSE (b). Time series of the model (red line) and observed (black dots) water elevation. (For interpretation of the references to colour in this figure legend, the reader is referred to the web version of this article.)

the maximum and minimum flooding extent from of the three most recent hydrological years covered by ALOS-2 PALSAR SAR data: 2014–2015, 2015–2016 and 2015–2017, with 50 m spatial resolution (available at https://www.mdpi.com/2072–4292/12/8/1326). These maps do not correspond to our simulation period (2007–2010), so three simulated periods of low water (November 1, 2007, 2008, and 2009) and high water (May 1, 2008, 2009, and 2010) were compared with the mapped areas. For this purpose, the fit metric (F, Eq. (1)) was used to determine the accuracy of the model (Schumann et al., 2009).

$$F = \left(\frac{a}{a+b+c}\right)100 \quad (1)$$

where a represents the total inundated area correctly mapped by the model (m^2), b is the inundated area not mapped by the model (underestimate; m^2), and c is the area not inundated and mapped by the model (overestimate; m^2).

Modeled flood extent maps were exported from the HEC-RAS model based on the DEM spatial resolution (30 m) as the model compares the computed water surface to the ground surface. Due to the different spatial resolutions of the flood extent products (HESS of 100 m, ALOS of 50 m, and modeled of 30 m), the fit metric was calculated after converting all raster maps to a vector format (ESRI shapefile), i.e., no raster resampling was performed.

The water surface elevation records observed at Óbidos and Curuai stations were considered for model validation (ANA operated stations; Location in Fig. 1). In addition, we used satellite altimetry data available for the main river considering 21 virtual stations spread along the river from the JASON2/JASON3 and ENVISAT satellites. These virtual stations are located at intersections of the altimeter track with the river and are available at https://hydroweb.theia-land.fr/ (Silva et al., 2010). Information for these stations can be found in Table A1 (Appendix). The model metrics evaluated were: i) RMSE, ii) Bias, iii) Pearson correction coefficient (r), and vi) Nash-Sutcliffe efficiency coefficient (NSE; Nash & Sutcliffe, 1970).

Finally, the Amazon River water flow was evaluated at Óbidos and Curuai floodplain. The Óbidos station continuously provides water level data and occasional flow measurements, in addition to the rating curve. Since no flow was measured between 2006 and 2010 at Óbidos, we used the rating curve for model validation, which may have large uncertainties (Filizola et al., 2014). In addition, we were able to obtain flow measurements in the Curuai floodplain during the 2006 flood season using a SonTek 1.5 MHz Mini Acoustic Doppler Current Profiler (ADCP) with errors smaller than 3%. Moving boat measurements were carried out with the Mini ADCP assembled on a home-built Catamaran platform integrated with a GPS. The ADCP platform was placed on the left side of the boat, near the bow, to avoid interference from the boat engine on measurements. The boat speed ranged from approximately 0.05 to 0.2 m s^{-1}. The same metrics for the water level were considered to evaluate the water flow.

3. Validation

3.1. Flood extent

The flood extent estimated by the ALOS product was 30 to 50% smaller than the area from the HESS product (Table 1). The ALOS product also hardly showed any interannual variability in flood extent between 2014 and 2017. Model performance was higher during the high water period (up to 82% for the HESS product) compared to the low water period (~50%). Although the metrics related to both products

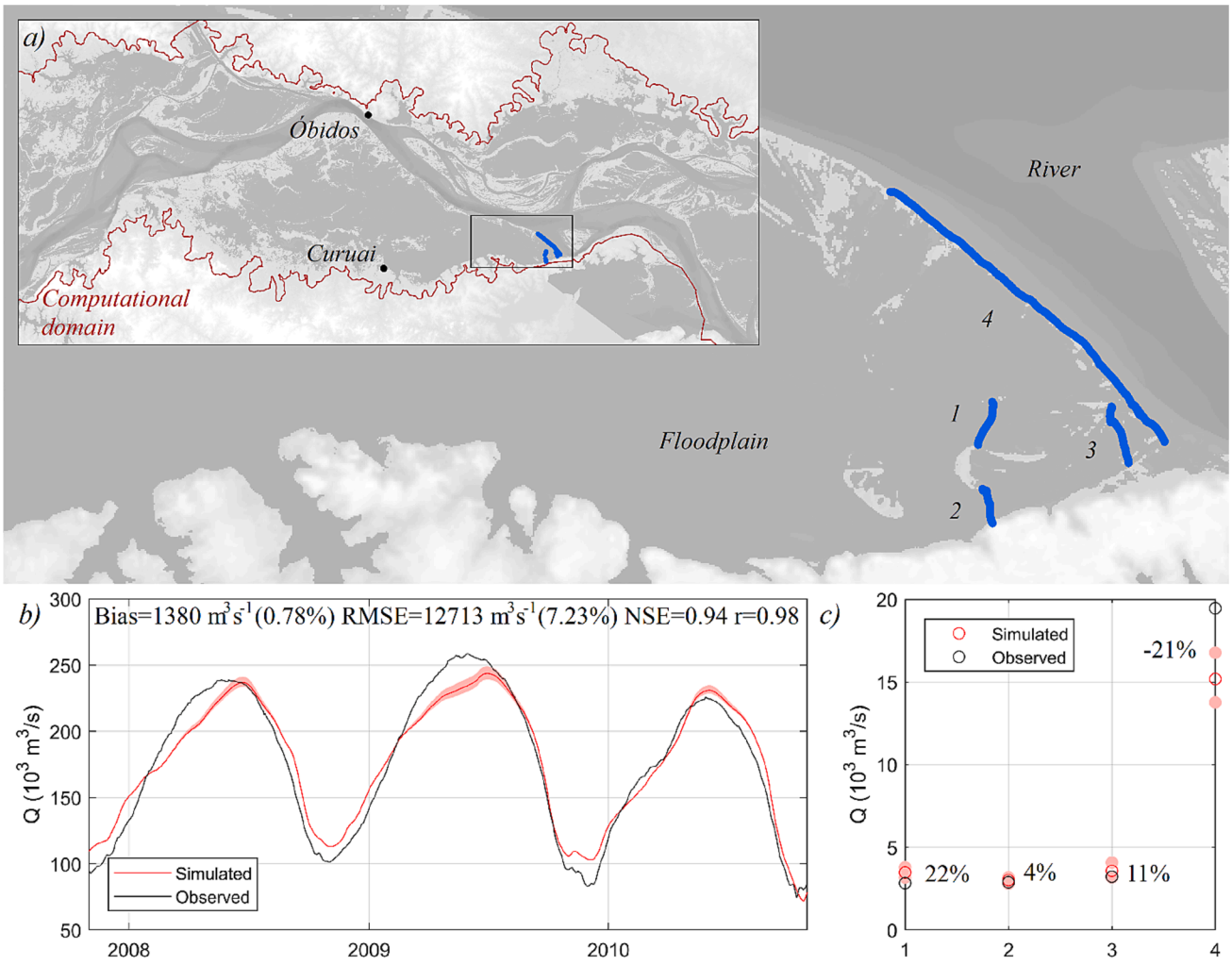

Fig. 4. Validation of water flow derived from the model (red line/dot with ± 30% perturbations in floodplain Manning coefficient) against observation (black line/dot) at Óbidos station (a) and in the floodplain on June 26, 2006 (b and c). Blue spots indicate location of ADCP profiles (1, 2, 3, and 4). (For interpretation of the references to colour in this figure legend, the reader is referred to the web version of this article.)

were similar at low water, there was more overestimation in simulated areas when compared to the ALOS product than when compared to the HESS product (see green areas in Fig. 2a). This was similar for the high-water period (see green areas in Fig. 2b), when the metrics for the HESS product (81–82%) was better compared to the ALOS product (56–58%). There was no significant variability in metrics among the years evaluated, indicating that discordance between simulated years (2007–2010) and observation years (1995–1996 and 2014–2017) was not as significant for validation as the product considered (HESS and ALOS).

Applications of hydrodynamic models to Amazon floodplains at different scales found fit metrics values ranging from 23% to 51% (low water) and 70% to 81% (high water) compared to the HESS map. de Paiva et al. (2013) represented the extent of large-scale flooding in the Amazon basin from the MGB model with values of 34% at low water and 70% at high water. Wilson et al. (2007) and Rudorff et al. (2014b) found values of 23 and 51% at low water and 72 and 81% at high water, respectively, in regional applications of the LISFLOOD-FP 2D model along the Amazon River reaches. Our model thus represented flood extent relatively well, with average F values of 52% in the low water period and 81–82% in the high-water period against the HESS map product. In addition, accuracy is of local relevance (F greater than 0.65) according to the criteria established by Fleischmann et al. (2019).

Errors in topographic mapping, the downstream boundary condition, and the lack of representation of hydrological processes in the floodplain, such as local infiltration, precipitation, evaporation and groundwater flow, can be sources of uncertainty in the flood extent mapping by the hydrodynamic model, especially in the low water period. In addition, it is noteworthy that the various remote sensing-derived water extent databases also have large inconsistencies among them. For example, Fleischmann et al. (2022) showed that HESS and ALOS mapping tend to underestimate the maximum inundation compared to subregional remote sensing-derived products, and there are large differences in minimum inundation among the different products.

Modelling lessons: 2D high resolution model improves the representation of flood extent compared to past modelling studies in the Amazon. Accuracy is usually better at high water than low water, while errors may be related to topography, local hydrological processes, and uncertainty of remote sensing maps.

3.2. Water surface elevation

Absolute water surface elevation in the river was well represented in the 23 stations evaluated (Table A3 in Appendix), with an average bias of −0.45 m, an RMSE of 0.77 m, an NSE of 0.87, and an *r* of 0.98 (Fig. 3). Only the stations monitored by ANA agency showed a positive bias (Óbidos and Curuai), while the altimetry stations consistently showed a negative bias. The highest RMSE (1.54 m) was observed at a station located in a channel with underestimation in the low water period

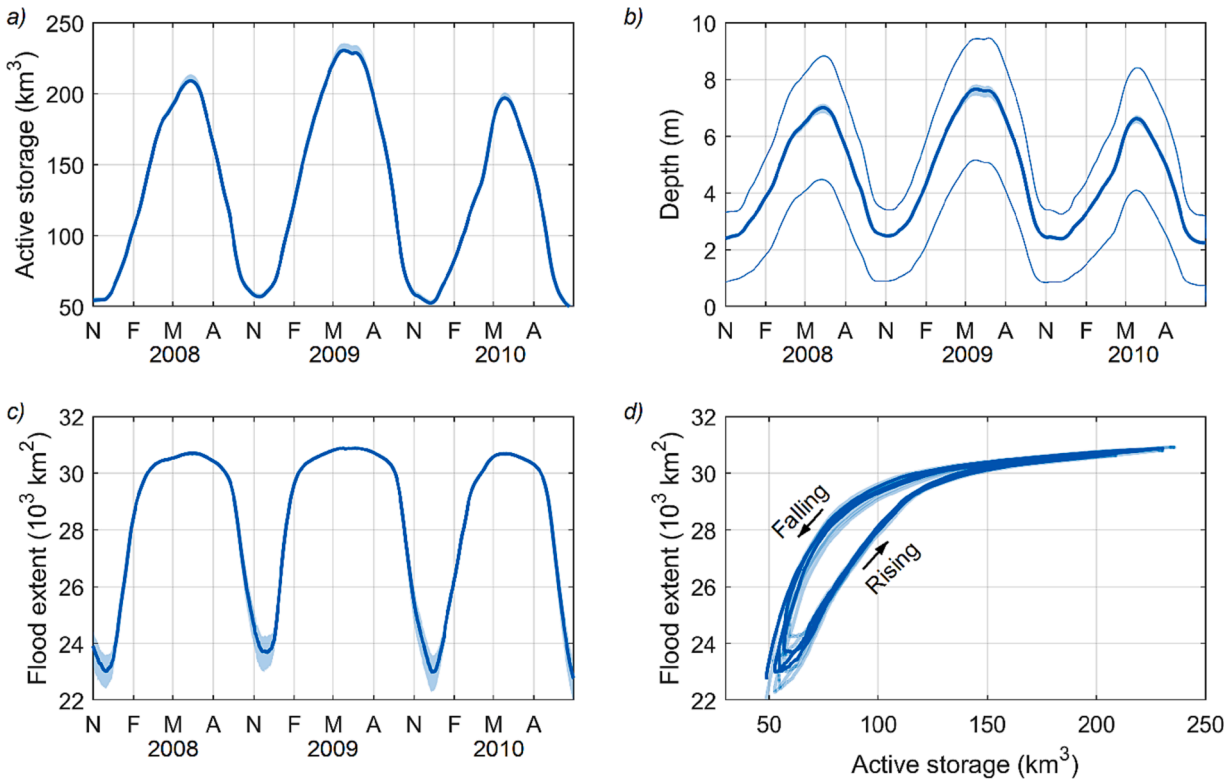

Fig. 5. Temporal series of a) active storage, b) average depth ± 25 and 75 percentile and c) flood extent in the floodplain. d) The relationship between active storage and flood extent in the floodplain. Transparent colors represent the simulations with ± 30% perturbations in floodplain Manning coefficient.

(Station 0392_01, Fig. 3b).

The errors were small in relation to the annual flood amplitude (4 to 10 m; Station 0063_01 and 0263_01 in Fig. 3a) and similar to the errors found by Wilson et al. (2007), which obtained an RMSE of 0.99 m at flood and 3.17 m at low water in the Amazon River. On the other hand, Rudorff et al. (2014b) found errors of 0.27 m at the Curuai station, considering the local hydrodynamic simulation of this floodplain using observed bathymetry. Our results also had a better agreement with observations compared to large-scale modeling in the Amazon basin. For instance de Paiva et al. (2013) obtained a NSE of 0.2–0.4 at Óbidos and Yamazaki et al. (2012b) obtained a NSE of 0.7 at Óbidos.

Modelling lessons: 2D high resolution model improves the representation of water surface elevation of the Amazon flood wave compared to past modelling studies. Error is small compared to the flood amplitude.

3.3. River and floodplain flow

The Amazon River discharge at Óbidos station was adequately represented by the model with a positive bias of 1380 m^3s^{-1} (0.78% of the mean observed discharge), an RMSE of 12,713 m^3s^{-1} (7.23% of the mean observed discharge), relatively high NSE = 0.94. No substantial alterations were observed in the modeling with ± 30% perturbations in Manning coefficient values in the floodplains. Values during the rising period (February to June) were underestimated, while during the rest of the year discharge values were slightly overestimated (Fig. 4a). It is likely that this underestimation is related to the uncertainties of the rating curve at Óbidos since it is calculated considering a single stage-discharge relationship, and/or errors in the boundary throughflows imposed in the model.

The observed flow was also evaluated across four transects located at the downstream outlet of the floodplain on June 26, 2006 (blue spots profiles in Fig. 4b and c). Despite the uncertainty of the bathymetry used in the simulation, the model adequately represented the flows on the floodplain, with differences from the observed flow ranging from −21% to 22% ($(Q_{mod} - Q_{obs})/Q_{obs}$). The flows in the three main channels (profiles 1, 2, and 3) were overestimated, while the flow in the longest profile was underestimated (profile 4). What is noteworthy about these measurements is the order of magnitude of the flows (ranging from 3000 to 19,000 m^3s^{-1}). The outflow on the floodplain in profile 4 represents 8.3% of the discharge observed at Óbidos on the same day (234000 m^3s^{-1}) and is greater than the average discharge of the Tapajós River (14500 m^3s^{-1}).

Modelling lessons: 2D high resolution model provides accurate representation of Amazon River discharge. Appropriate representation of expressive floodplain flow with errors smaller than 20%.

4. Flood dynamics on the floodplain

4.1. volume, depth, and flood extent

In the low water period (November), the volume stored in the floodplains ranged from 55.3 km^3 (2010) to 59.68 km^3 (2009), while in the high water period (June), the volume stored ranged from 204 km^3 (2010) to 238 km^3 (2009) (Fig. 5a). Therefore, the floodplain has an average volume variation of 162 km^3, i.e., annually, this volume is stored and then drained from the floodplain between low water and flood periods. The volume stored annually in the central Amazon floodplain (162 km^3) represents about 2.8% of the Amazon River volume exported to the ocean annually. That annual variation is larger than the estimated over the open-water floodplains of the central Amazon (116 km^3; Fassoni-Andrade et al., 2020a) and smaller than the estimate over the Amazon floodplains in six square regions of 330 km × 330 km (285 km^3; Alsdorf et al., 2010). It represents 13.5% (Papa et al., 2013) to 18% (Frappart et al., 2019) of the total surface water storage at the Amazon basin scale estimated by remote sensing data. Furthermore, the estimated volume stored in the floodplain showed a difference of 34 km^3 at the flood peak between years characterized by large (2009) and small (2010) flood. This volume is significant and represents 20% of the

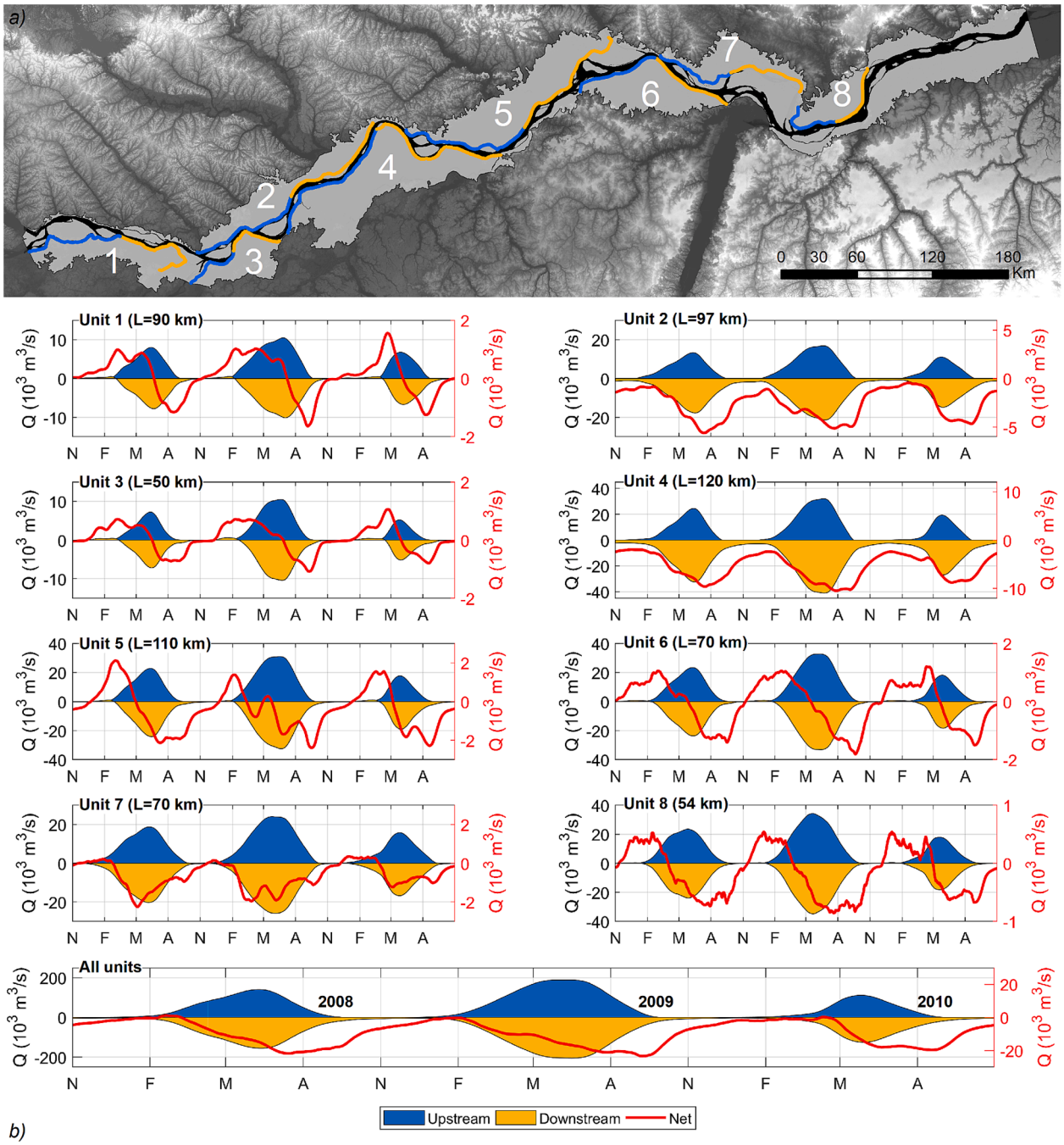

Fig. 6. (a) Map and (b) temporal series of water flow in eight floodplain units from 2008 to 2010. Blue and yellow transects represent, respectively, the upstream and downstream region of each unit (left y-axis), and the red line represents the resulting net flow (right y-axis). Note the widely different scales in left and right y-axes. (For interpretation of the references to colour in this figure legend, the reader is referred to the web version of this article.)

annual volume variation and 60% of the average volume stored in the floodplain during the low water period.

Lesson 1: Annual volume variation of 160 km^3 in the central Amazon floodplain. Variation represents about 3% of the Amazon River volume exported to the ocean annually. Large and small floods cause interannual variability of 20% in volume variation.

Water depth in the floodplain showed a similar pattern to that of the stored volume (Fig. 5b), with an average depth of 4.62 m, i.e., the average depth ranges from 2.5 m to 7.12 m between the low water and high water periods. The average depth variation in the flood period was 40 cm lower in the dry year (2010) and 60 cm higher in the wet year (2009) compared to a normal year (2008). These values can be significant when considering the amplitude of the water level, which varies from 10 m upstream to 4 m downstream reach (Fassoni-Andrade et al., 2020a). Furthermore, the variation of 1 m between extreme floods (2009 and 2010) represents 22% of the annual variation of the average depth.

Lesson 2: Average water depth in the central Amazon floodplain ranges from 2.5 to 7.1 m annually. Large and small floods cause variations of up to 1 m at high water or 22% of the annual variation.

The flood extent showed an average value of 31500 km^2 and 23940 km^2 during the high water and the low water periods, respectively (Fig. 5c), i.e., an annual variation of 7560 km^2. These values represent, respectively, 5% and 8% of the mapped wetlands in the Amazon basin during the high and low water periods (Hess et al., 2015). However, in contrast to the strong interannual variation in stored volume, the flood

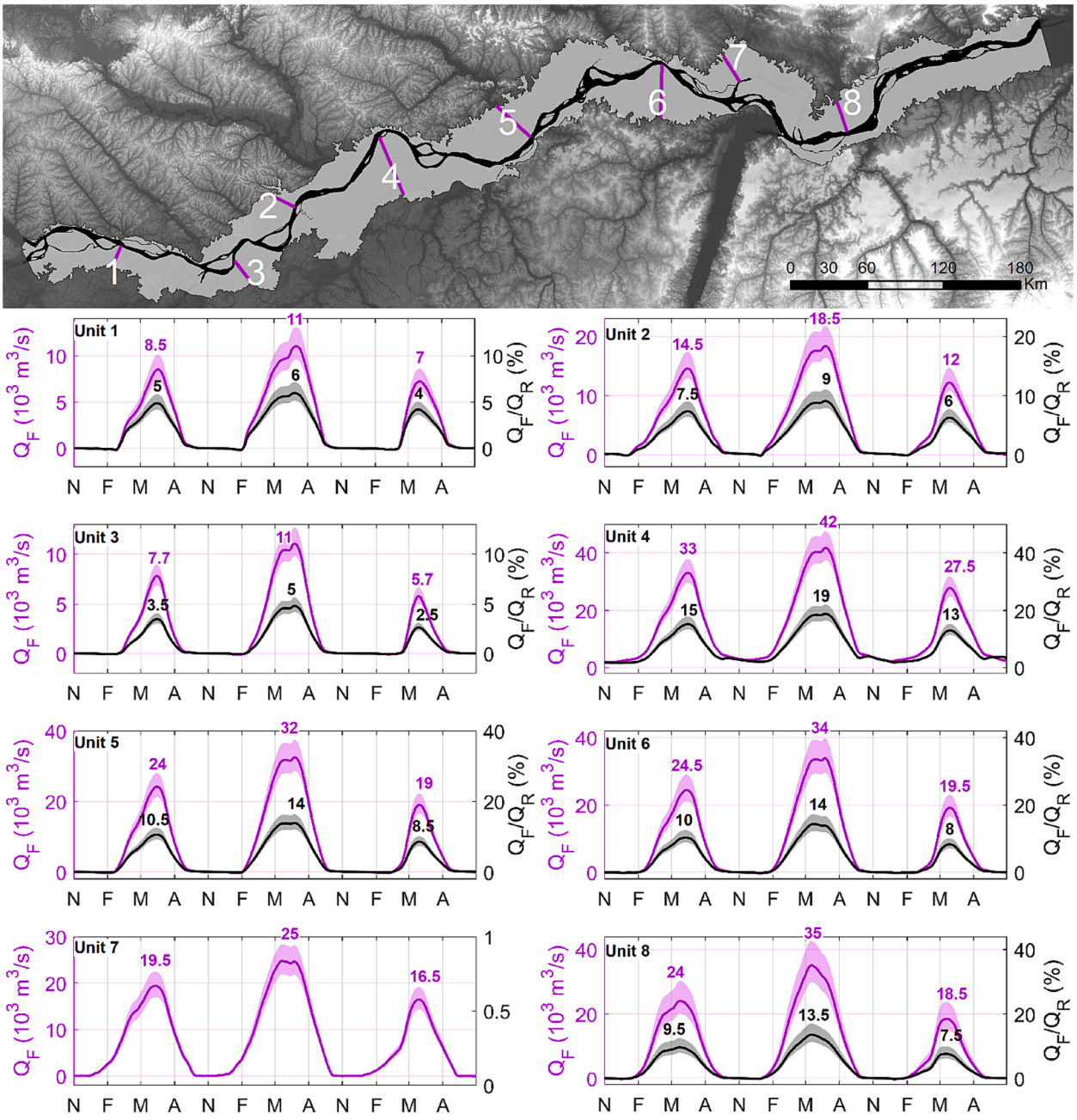

Fig. 7. (a) Map and (b) temporal series of transverse flows in the floodplain in the eight units (purple; left y-axis) and the percentage of flow in the transverse transect (Q_F) relative to the river discharge (Q_R) (black; right y-axis) from 2008 to 2010. Transparent colors represent the simulations with ± 30% perturbations in floodplain Manning coefficient. Q_F/Q_R was not evaluated in unit 7. (For interpretation of the references to colour in this figure legend, the reader is referred to the web version of this article.)

extent presented a plateau during the high water period with differences of ~ 200 km^2 between 2009 and 2010, which represents only 2.6% of the average variation between high and low water periods. This means that flood intensity does not have such a large impact on flood extent (2.6%) compared to its impact on volume (20%) and on water depth (22%). The flood extent finds a plateau during the flood possibly due to topographic constrains limited by the geomorphology of the Amazon River and the Uplands at the floodplain boundaries.

Lesson 3: Annual flood extent variation of 7560 km^2 in the central Amazon floodplain. Large and small floods cause interannual variability of only 3% in flood extent variation. Flood extent presents a plateau in extreme floods, possibly due to topographic constrains.

The relationship between volume and flood extent on the floodplain indicates a counter-clockwise hysteresis, as also documented by Rudorff et al. (2014b) for Curuai floodplain, i.e., for the same stored volume, the flood extent is larger in the falling than in the rising period (Fig. 5d). For example, the flood extent was 29500 km^2 in the falling period and 28000 km^2 in the rising period for a stored volume of 100 km^3. This may be related to the floodplain hydrodynamic complexity, as the asymmetry of the Amazon River hydrograph, where the rising period is slower than the falling period (Fleischmann et al., 2016), the reversal of river-floodplain surface water slope (Zhang and Werner, 2015), or the time taken for water to fill deeper parts of the floodplain before flooding upper regions.

Lesson 4: Significant flood extent and volume hysteresis that may be related to the floodplain hydrodynamic complexity.

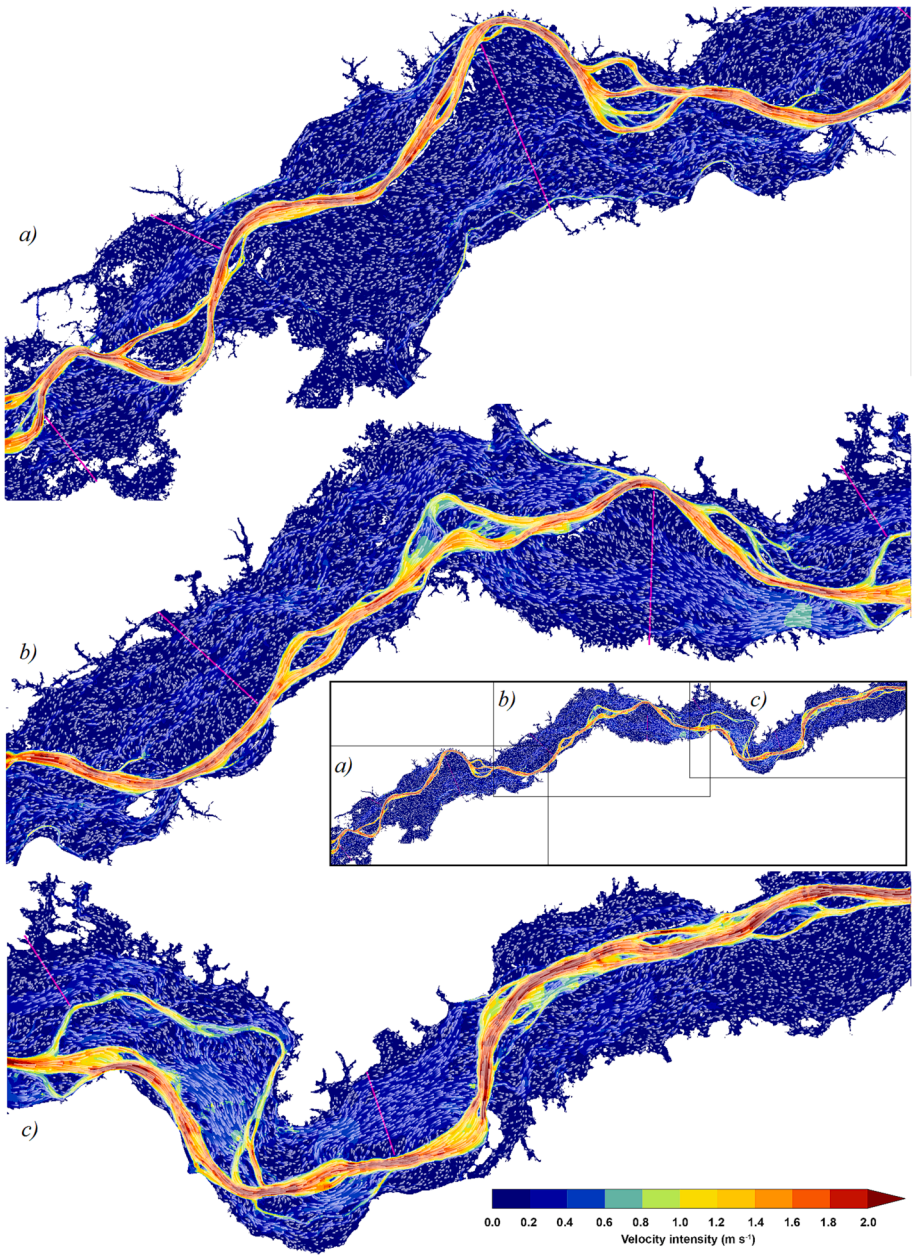

Fig. 8. Map of water velocity field in the floodplain during the flood period (June 15, 2009). The blue to red colorbar indicates the velocity intensity (m s^{-1}) and the white streamlines the flow direction. The panels are a continuous sequence of the study area, as seen in the inset. (For interpretation of the references to colour in this figure legend, the reader is referred to the web version of this article.)

4.2. River-floodplain flow exchange

The water exchange between the Amazon River and the floodplain was evaluated in eight units by estimating the flow across transects parallel to riverbanks. In each unit, two transects of equal length (L) were defined: one upstream and one downstream. These transects consider that most of the water inflow (outflow) in the floodplain occurs in the upstream (downstream) half. However, dominant inflow/outflow boundaries have not been defined. In the Curuai floodplain (Unit 6), for example, water outflow is predominantly in a smaller downstream transect (Rudorff et al., 2014a).

Fig. 6 shows the flows across both transects (blue and yellow), and the resulting net flow (red line). Positive values indicate that the floodplain is receiving water from the river (inflow), and negative values indicate that water is flowing out of the floodplain (outflow). Since our model does not consider infiltration, precipitation, evaporation and groundwater flow, the net flow is the result of the discharge received from the tributaries. These processes have a minor impact on the inputs of water to the floodplain, as shown for Lago Grade de Curuai floodplain (location in Fig. 4a), where rainfall and runoff accounted for about 9% and 10% of the annual total inputs, while seepage from the groundwater system accounted for 4% (Bonnet et al., 2008).

In all units, the inflow and outflow of water from the floodplain predominates, respectively, in the upstream and downstream transect, i.e., inflow or outflow can occur in both transects, but the balance is positive (negative) for the upstream (downstream) transect. In general, the inflow in the floodplain begins with the river flood and predominates until the flood peak (May/June/July). During the falling period, outflow becomes predominant with a maximum in August/September, when there is little or no inflow to the floodplain. Floodplain flow drainage (outflow) continues to occur in the units with small values until the onset of the flood. In regions 2 and 4, the outflow is greater in the low

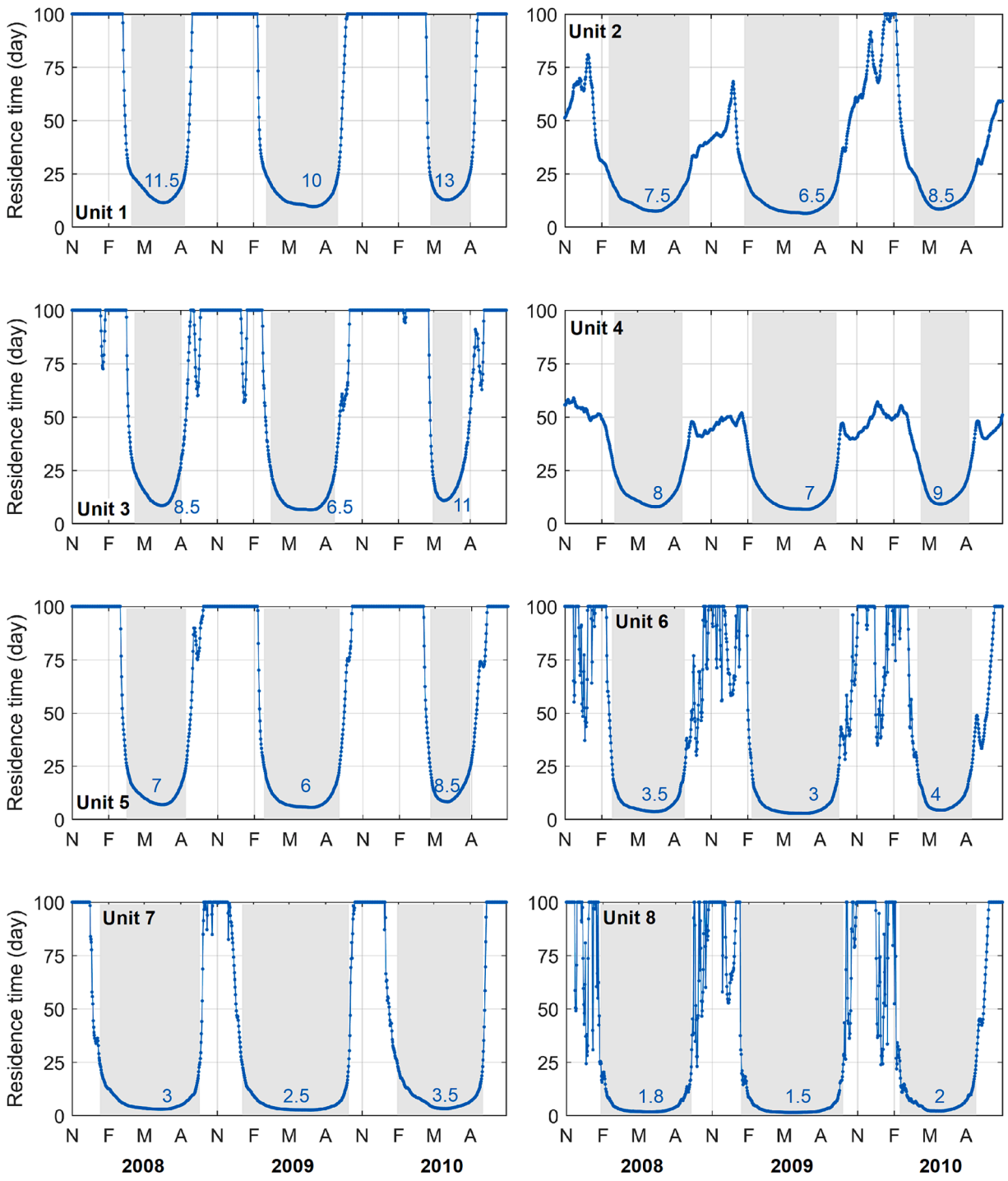

Fig. 9. Temporal series of water residence time in the eight units from 2007 to 2010 (restricted to values smaller than 100 days for clarity). Blue labels represent the minimum observed during the flood and gray regions represent the high water renewal period, defined as the period in which the residence time is less than or equal to 25 days. (For interpretation of the references to colour in this figure legend, the reader is referred to the web version of this article.)

water period due a significant flow contribution from the tributaries.

The water exchange between the river and the floodplain during the flood is very intense with inflows and outflows ranging from 5500 to 35000 $m^3 s^{-1}$ (units 3 in 2010 and 8 in 2009, respectively). However, these values represent the inflow and outflow occurring practically at the same time in the units (gross flows in blue and yellow lines in Fig. 6), greatly surpassing the net inflow and outflow (red line in Fig. 6) and indicating weak water storage in the floodplain.

Lesson 5: Gross flow greatly surpasses the net inflow and outflow in the floodplain units during the flood, indicating that the floodplain flux is generally more expressive than storage infilling and outfilling.

In units 1, 3, 5, and 6, flooding begins between February and April, depending on the year: March in 2008, February in 2009, and April in 2010. That is, a small flood and a large flood cause, respectively, a delay and an advance of the water inflow into the floodplain by approximately one month in these units. These findings are similar to results for Lake Janauacá in central Amazon (Pinel et al., 2019). Inflow onset in units 2, 4, 7, and 8 occurs in December/January regardless of the year, therefore, these areas seem to have more connection with the river from channelized flows. Although the positive balance is initiated in different

Table A1
Name, code, and location of in situ stations operated by Agência Nacional de Águas e Saneamento Básico (ANA) and virtual stations (available in Hydroweb; https://www.theia-land.fr/).

Name	Code	Source	Latitude	Longitude
Manacapuru	14100000	ANA	−3.308	−60.609
Porto de Moz	18950003	ANA	−1.753	−52.241
Moura	14840000	ANA	−1.456	−61.634
Jatuarana	15030000	ANA	−3.052	−59.678
Parintins	16350002	ANA	−2.630	−56.752
Santarém	17900000	ANA	−2.416	−54.716
Curuai	17060000	ANA	−2.268	−55.481
Óbidos	17050001	ANA	−1.947	−55.511
amz_amz_env_	0020_01	Hydroweb	−3.161	−59.465
amz_amz_env_	0063_01	Hydroweb	−3.338	−58.774
amz_amz_env_	0220_01	Hydroweb	−2.391	−54.266
amz_amz_env_	0263_01	Hydroweb	−2.083	−54.020
amz_amz_env_	0306_01	Hydroweb	−1.907	−55.596
amz_amz_env_	0349_01	Hydroweb	−1.946	−55.487
amz_amz_env_	0392_01	Hydroweb	−2.533	−57.171
amz_amz_env_	0435_01	Hydroweb	−2.611	−56.778
amz_amz_env_	0478_02	Hydroweb	−3.331	−58.784
amz_amz_env_	0521_01	Hydroweb	−2.953	−58.14
amz_amz_env_	0607_01	Hydroweb	−3.125	−59.539
amz_amz_env_	0764_01	Hydroweb	−2.146	−54.930
amz_amz_env_	0807_01	Hydroweb	−2.405	−54.668
amz_amz_env_	0850_01	Hydroweb	−2.368	−56.416
amz_amz_env_	0893_01	Hydroweb	−2.123	−56.167
amz_amz_env_	0936_01	Hydroweb	−2.798	−57.948
amz_amz_env_	0979_01	Hydroweb	−2.407	−57.542
R_amz_amz_jas_	0139_01	Hydroweb	−2.571	−56.897
R_amz_amz_jas_	0152_01	Hydroweb	−3.254	−59.068
R_amz_amz_jas_	0228_01	Hydroweb	−2.488	−56.508
R_amz_amz_jas_	0063_01	Hydroweb	−3.281	−59.985

months in the units, the maximum inflow and outflow occurs at the time of river peak flood (June/July), since diffuse overbank throughflow in the floodplain predominates.

Lesson 6: Extreme floods can offset by one month the timing of the floodplain inflow onset (delay and advance). No interannual variability in the timing of the maximum flood.

The total water inflow considering all units (area of 40000 km^2) is maximum during the 2009 flood with values of 189600 m^3 s^{-1}, representing more than the peak flood of the Solimões River in the same year for instance (~160000 m^3 s^{-1}). On the other hand, the outflow from the floodplain is 206000 m^3 s^{-1} in the 2009 flood. These values are much lower at the peak of the 2010 weak flood: the maximum inflow and outflow are respectively to 60% and 62% of the values in 2009. Therefore, an large (small) flood promotes a 33% (22%) increase (decrease) in floodplain net flow during the flood compared to a more normal year (e.g., 2008, when 142700 m^3 s^{-1} are seen).

Lesson 7: Variations in flood duration in extreme floods can induce a 33% (22%) increase (decrease) in floodplain net flow.

4.3. Riverine fluxes over floodplain units

Fig. 7 shows the transverse flows across the sections in the floodplain units (purple; left y-axis) and this flow (Q_F) expressed as a percentage of the Amazon River discharge (Q_R) (black; right y-axis) for 2008, 2009, and 2010.

Flows along the transverse profiles are towards downstream during the flood (positive values in the graphs) and broadly parallel to the river, as can be seen in Fig. 8 for the 2009 flood. During 2008 (normal year), floodplain flows vary from 7700 to 33000 m^3 s^{-1} (units 3 and 4) representing from 3.5% to 15% of the Amazon River discharge (average of 8.7%). During large and small floods, flows vary from 5% to 19% (2009) and from 2.5% to 13% (2010) of the Amazon River discharge, respectively. These values are very significant, as they are similar in magnitude to the average discharge of the largest tributaries of the Amazon River (e.g., 28000 m^3 s^{-1} for the Negro River and 31000 m^3 s^{-1} for the Madeira River). As these flows are not stored in the floodplain (inflow and outflow occur roughly at the same time; Fig. 6), the eight units behave as very active zones with riverine fluxes during the flood. Furthermore, the Amazon River can be considered not only as the most voluminous river in the world (Callède et al., 2010) but also as the widest during the flood (ranging from 21 km to 54 km wide), since the floodplain units can be considered as an active extension of the river.

Lesson 8: Amazon floodplain units convey large amounts of riverine fluxes with flows up to 20% of the Amazon River discharge, the most voluminous river in the world.

During the low water period, the flow in the cross transects is

Table A3
Water surface elevation metrics evaluated at Amazon River stations.

Station	Number of data	Bias	RMSE	NSE	*r*
0020_01	28	−0.86	1.38	0.82	0.94
0063_01	29	−0.43	0.58	0.97	1.00
0220_01	29	−0.42	0.48	0.93	0.99
0263_01	30	−0.40	0.48	0.92	0.99
0306_01	31	−0.60	1.01	0.83	0.95
0349_01	29	−0.47	0.62	0.93	0.99
0392_01	31	−1.28	1.54	0.61	0.95
0435_01	30	−0.47	0.62	0.95	0.99
0478_02	31	−0.36	0.51	0.98	1.00
0521_01	30	−0.48	0.61	0.96	0.99
0607_01	29	−0.13	0.45	0.99	0.99
0764_01	29	−0.59	0.70	0.85	0.98
0807_01	29	−0.82	1.02	0.64	0.96
0850_01	31	−0.59	0.67	0.94	1.00
0893_01	31	−0.83	0.99	0.84	0.98
0936_01	29	−0.75	0.80	0.93	1.00
0979_01	31	−0.47	0.68	0.95	0.99
0139_01	81	−0.68	1.38	0.45	0.95
0152_01	75	0.00	0.61	0.96	0.98
0228_01	82	−0.50	0.94	0.81	0.97
0063_01	74	−0.15	0.64	0.98	0.99
Curuai	1005	0.65	0.67	0.92	1.00
Óbidos	1066	0.30	0.37	0.98	1.00

Table A2
Manning's roughness coefficients adopted in each class of the mapping of Hess et al. (2015) and proportion of the area occupied in the computational domain.

Class	Description (Hess et al., 2003)	Mapping code (Hess et al., 2015)	Manning's roughness coefficients	Spatial proportion in the domain*
Open water	Lago, paraná, igarapé, furo	11 13	0.022 (Same as the river)	17%
Bare soil or herbaceous	Terreno aberto, campo, macrófitas aquáticas	21 23 33	0.03	18%
Shrub	Vegetação arbustiva, campina	41 44 45 51 55	0.04	11%
Woodland	Chavascal, pântano, savanas inundadas	66 67 77	0.14	27.3%
Forest	Floresta, mata	88 89 99	0.14	4.4%
Terra firme	Outside of the floodplain	–	0.18	9.1%

*13.2% of the area represents the Amazon River.

significantly weaker and may occur in the opposite direction, towards upstream (negative values in Fig. 7). These reverse flows in February 2009, for example, ranged from 76 $m^3 s^{-1}$ to 389 $m^3 s^{-1}$ (units 3 and 6). This is also observed in the downstream transects with positive values in Fig. 6 (yellow transects), i.e., there is an inflow in the floodplain in the downstream region during the low-water period, predominantly in February.

Velocity fields in the floodplain are spatially heterogeneous with regions of more active flows in channels and storage areas that can be disconnected from the Amazon River (Fig. 8). These velocity fields confirm that water inflows and outflows on the floodplain occur predominantly in the upstream and downstream regions of the floodplain, respectively, and the floodplain is fragmented into units bounded by the river geomorphology with constant inflows and outflows from the floodplain.

Lesson 9: Spatial and temporal heterogeneity in floodplain velocity fields with active flow and storage areas. Velocity fields confirm that the central Amazon floodplain is fragmented into units with significant water inflow/outflow to/from the main river.

The estimation of the amount of water exchanged between the Amazon River and the floodplain differs from previous studies. From the water balance of six regions along the Amazon River using remote sensing observations, Alsdorf et al. (2010) showed that the filling or drainage of the floodplain accounts for no more than 10% of the river discharge during any time in the regions evaluated. On the other hand, Richey et al. (1989) estimated that up to 30% of the Amazon River discharge is exchanged with the floodplain using water balance and a simplified routing propagation method (Muskingum-Cunge). Getirana et al. (2012) showed much lower values using a global-scale flow routing scheme, with a mean of 2.3% and a maximum of 4% in central Amazon. Our findings showed that from 3.5% to 15% of the Amazon River flow passes through the floodplain during a moderate flood but can reach 20% during an large flood. Furthermore, floodplain flows are not greatly altered with ± 30% perturbations in floodplain Manning coefficient (transparent colors in Fig. 7). Although our results are, respectively, larger and lower than Getirana's and Richey's estimates, the two-dimensional hydrodynamic modeling approach performed in this study is the only one that allowed direct estimates of gross floodplain flows.

4.4. Residence time

Water residence time in the floodplain units, i.e., the ratio of water volume to net flow, can be clearly divided into two periods in the eight units: one of high water exchange of the floodplain with the river during the flood (gray regions in Fig. 9) and one of low water exchange during the low water. Water renewal in the flood season (April/May/June) is high with residence time values ranging from 1.5 to 13 days (units 8 and 1, respectively) with an average of 6.4 days for all units. After the flood, residence time increases rapidly in the falling period (August/September/October) to values greater than 100 days at low water (November to January), which represents a condition at a given instant, i.e., a theoretical steady-state condition that does not actually occur. In the units 2 and 4, residence time at low water remains shorter, as it varies between 50 and 75 days due to the greater contribution of tributaries. These estimates are global at the scale of the floodplain units, but the residence time may vary within a given floodplain, especially in the low water period, among regions of swift current, such as channels connected to the river, and slower flow regions, such as lakes disconnected from the drainage network.

Lesson 10: Water renewal in the floodplain units is high (low) during high water (low water) with water residence time around 6 days during high water and several months during low water period.

The duration of the high water renewal period, defined here as the period in which the residence time is less than or equal to 25 days (gray regions in the Fig. 9), has an average of 177 days across all units. In units 1, 3 and 5, this period varies between 100 and 150 days. In units 2, 4 and 6 the duration is 150 to 200 days, and in units 7 and 8 the duration is 200 to 250 days. Therefore, there appears to be an increase in the period of high water renewal from upstream to downstream floodplains units.

Lesson 11: Period of high water renewal in the central floodplain units increases from upstream to downstream of the Amazon River.

The mean residence time in 2008 was 6.4 days with the high water renewal period lasting 6 months (179 days), whereas in 2009 and 2010, the mean residence time was 5.4 and 7.4 days with high water renewal period of 215 and 137 days, respectively. Thus, an large (small) flood appears to promote a shorter (longer) average residence time of approximately 1 day and a longer (shorter) high water renewal period between the river and the floodplain of approximately 40 days. This is in line with section 4.2, in which an large (small) flood causes an advanced (a delay) of the water inflow into the floodplain by approximately one month.

Lesson 12: large and small floods cause variations of up to 80 days in the duration of the period of high water renewal.

5. Summary and conclusions

In this study we present the results of the first ever high resolution 2D hydrodynamic simulation of water flows over a large area (40000 km^2) in the central Amazon floodplain, covering a three-year period (2007–2010) including normal, large and small flood years. The model improved the representation of water surface elevation of the Amazon River and flood extent in the floodplain compared to past modelling studies. The study also provides significant advances over previous local scale (small area) studies. Model accuracy for flood extent was better in high water conditions (~80%) than in low water conditions (~52%) and the error in water surface elevation (77 cm) was small compared to the Amazon flood amplitude. The model also provided accurate representation of floodplain flow and Amazon River discharge with errors smaller than 20%.

Part of the modelling errors may be related to model input and validation data, such as remote sensing maps of water surface extent, and the lack of representation of hydrological processes, such as local infiltration, precipitation, evaporation and groundwater flow. Uncertainties in the model input discharge are small (about 4% at Manacapuru station and 15% for MGB model; Alves et al., 2021; Siqueira et al., 2018) and have minor impact on our findings. Despite the small vertical error of the topographic data (90 cm), permanently flooded areas in the floodplain are underestimated, causing uncertainties in our results (depth and volume), especially in the low water period. Similarly, the water level used as a downstream boundary condition was obtained at a gauge station 77 km downstream that possibly has a smaller flood pulse amplitude (about 40 cm lower) and therefore causing uncertainty in the model, especially in downstream floodplain units and in low water period (overestimated minimum level). Finally, simple uncertainty analysis of the sensitivity of the modelling to the Manning coefficient in the floodplain, which is probably the most uncertain parameter in the model, showed robust results in floodplain flows, with minor impact on our conclusions. The representation of hydrological processes in the floodplain should be further evaluated in future studies since these processes can affect the residence time and water flow in the floodplain (e.g. Tull et al., 2022).

The stored volume, average depth, and flood extent in the floodplain varied on average by 162 km^3, 4.6 m (2.5 to 7.1), and 7560 km^2 respectively, between the low and high water periods (*Lessons 1, 2, 3*; hereafter *L*). The floodplain can be compared with a confined basin in which large and small floods, such as that of 2009 and 2010, have more impact on the stored volume and water depth in the floodplain than on the flood extent (*L3*). We observed significant flood extent and volume hysteresis that may relate to the floodplain hydrodynamic complexity (*L4*).

Gross inflow and outflow in floodplain units greatly surpass the net

inflow and outflow, indicating that the floodplain flux is generally more expressive than storage infilling and outfilling (*L5*). Large and small floods can promote an advance or delay, respectively, of up to one month in the flood onset in some floodplain units, although the peak occurs in the same period of the river flood (May and June; *L6* and *L7*).

For the first time, our results show how the Amazon River floodplains are intensely active during the flood (May/June), with parallel riverine fluxes in floodplain units ranging from 2.5% to 20% of the main river discharge in the same period (*L8*) and water residence time ranging from 1.5 to 13 days (*L10*). This indicates that the Amazon floodplains route a large fraction of the riverine fluxes. If we consider the floodplains (20–50 km wide) as a continuous extension of the river channel the Amazon River is the widest river in the world during the flooded season. Conversely, the water residence time can be of several months during the periods of low water renewal with the river, and low water floodplain flows show negligible values when compared to the flood period. The floodplain velocity fields are heterogeneous, with active flow channel and storage areas (*L9*). Furthermore, large and small floods promote, respectively, an increase and decrease of duration of the high water renewal period by 40 days due to the advance and delay of water inflow into the floodplain (*L11* and *L12*).

Our study contributes to understanding the dynamics of the complex Amazon hydrological systems. The 12 learned lessons about the Amazon floodplain hydrodynamics have important implications. For example, the rating curves used to monitor the Amazon River discharge at Óbidos, the lowermost hydrological gauge station in the voluminous Amazon River, do not account for the flow that passes through the floodplain - about 14% in the 2009 flood (34000 $m^3 s^{-1}$). This flow rate is larger than the average discharge of the largest tributaries of the Amazon River (e.g., 28000 $m^3 s^{-1}$ for the Negro River and 31000 $m^3 s^{-1}$ for the Madeira River). Therefore, estimates that depend on the river discharge, such as export of water (Callède et al., 2010), carbon (Richey et al., 2022) and sediment to the ocean (Armijos et al., 2020), water balance (Moreira et al., 2019), and even climate assessment (Jahfer et al., 2017) may be biased. Our findings are also important to understand the impacts of large floods, that have been recently more frequent in central Amazon (Chevuturi et al., 2022), on riparian communities, improve the representation of hydrodynamic processes in floodplains in larger-scale models (e.g. MGB and Camaflood), mapping aquatic habitats (Hess et al., 2015), and understand nutrient and sediment budgets in the floodplain, since the water mixing strongly influences the biogeochemical characteristics of the water (Wohl, 2021).

Declaration of Competing Interest

The authors declare that they have no known competing financial interests or personal relationships that could have appeared to influence the work reported in this paper.

Data availability

Data will be made available on request.

Acknowledgments

The authors would like to thank Conrado Rudorff and Walter Collischonn for their insights. This research is supported by CNPq (Conselho Nacional de Desenvolvimento Científico e Tecnológico; 140352/2016-3) and CAPES (Coordenação de Aperfeiçoamento de Pessoal de Nível Superior; 88881.697095/2022-01). This research is funded through the BNP Paribas foundation under the 2019 Biodiversity & Climate Initiative programme and the 2017-2018 Belmont Forum and BiodivERsA joint call for research proposals, under the BiodivScen ERA-Net COFUND programme, and with the funding organisations French National Research Agency (ANR), São Paulo Research Foundation (FAPESP), National Science Foundation (NSF), the Research Council of Norway and the German Federal Ministry of Education and Research (BMBF).

ACFA and RP designed the experiments. ACFA developed the model and performed the simulations. All authors contributed to the draft by providing input for the final manuscript and discussion of the results.

Appendix

Table A1.
Table A2.
Table A3.

References

Abril, G., Martinez, J.M., Artigas, L.F., Moreira-Turcq, P., Benedetti, M.F., Vidal, L., Meziane, T., Kim, J.H., Bernardes, M.C., Savoye, N., Deborde, J., Souza, E.L., Albéric, P., Landim De Souza, M.F., Roland, F., 2014. Amazon River carbon dioxide outgassing fuelled by wetlands. Nature 505, 395–398. https://doi.org/10.1038/nature12797.

Alsdorf, D., Rodriguez, E., Lettenmaier, D.P., 2007. Measuring surface water from space. Rev. Geophys. 45, 1–24. https://doi.org/10.1029/2006RG000197.1.INTRODUCTION.

Alsdorf, D., Han, S.C., Bates, P., Melack, J., 2010. Seasonal water storage on the Amazon floodplain measured from satellites. Remote Sens. Environ. 114, 2448–2456. https://doi.org/10.1016/j.rse.2010.05.020.

Alsdorf, D., Beighley, E., Laraque, A., Lee, H., Tshimanga, R., O'Loughlin, F., Mahé, G., Dinga, B., Moukandi, G., Spencer, R.G.M., 2016. Opportunities for hydrologic research in the Congo Basin. Rev. Geophys. 54, 378–409. https://doi.org/10.1002/2016RG000517.

Alves, L.G.S., da Silva, D.D., Vauchel, P., Fraizy, P., Filizola, N.P., 2021. Variable backwater and channel roughness: Effects on Solimões River discharge. Comptes Rendus - Geosci. https://doi.org/10.5802/CRGEOS.35.

Arcement Jr, G.J., Schneider, V.R., 1989. Guide for Selecting Manning's Roughness Coefficients for Natural Channels and Flood Plains. Tech. Report, Geol. Surv. Water-Supply, United States Gov. Print. Off. Washington, U.S.A 38. Report No. FHWA-TS-84-204.

Armijos, E., Crave, A., Espinoza, J.C., Filizola, N., Espinoza-Villar, R., Ayes, I., Fonseca, P., Fraizy, P., Gutierrez, O., Vauchel, P., Camenen, B., Martiınez, J.M., Dos Santos, A., Santini, W., Cochonneau, G., Guyot, J.L., 2020. Rainfall control on amazon sediment flux: Synthesis from 20 years of monitoring. Environ. Res. Commun. 2, 051008 https://doi.org/10.1088/2515-7620/ab9003.

Barbosa, C.C.F., Novo, E.M.L. de M., Melack, J.M., Freitas, R.M. de, Pereira, W., 2006. A methodology for analysis of volume and flooded area dynamics: Lago Grande de Curuai várzea as an example. Rev. Bras. Cartogr. 58, 201–210.

Basso, L.S., Marani, L., Gatti, L.V., Miller, J.B., Gloor, M., Melack, J., Cassol, H.L.G., Tejada, G., Domingues, L.G., Arai, E., Sanchez, A.H., Corrêa, S.M., Anderson, L., Aragão, L.E.O.C., Correia, C.S.C., Crispim, S.P., Neves, R.A.L., 2021. Amazon methane budget derived from multi-year airborne observations highlights regional variations in emissions. Commun. Earth Environ. 2, 1–13. https://doi.org/10.1038/s43247-021-00314-4.

Baugh, C.A., Bates, P.D., Schumann, G., Trigg, M.A., 2013. SRTM vegetation removal and hydrodynamic modeling accuracy. Water Resour. Res. 49, 5276–5289. https://doi.org/10.1002/wrcr.20412.

Beighley, R.E., Eggert, K.G., Dunne, T., He, Y., Gummadi, V., Verdin, K.L., 2009. Simulating hydrologic and hydraulic processes throughout the Amazon River Basin. Hydrol. Process. 23, 1221–1235. https://doi.org/10.1002/hyp.

Birkett, C.M., Mertes, L.A.K., Dunne, T., Costa, M.H., Jasinski, M.J., 2002. Surface water dynamics in the Amazon Basin: Application of satellite radar altimetry. J. Geophys. Res. D Atmos. 107 https://doi.org/10.1029/2001JD000609.

Bonnet, M.P., Barroux, G., Martinez, J.M., Seyler, F., Moreira-Turcq, P., Cochonneau, G., Melack, J.M., Boaventura, G., Maurice-Bourgoin, L., León, J.G., Roux, E., Calmant, S., Kosuth, P., Guyot, J.L., Seyler, P., 2008. Floodplain hydrology in an Amazon floodplain lake (Lago Grande de Curuaí). J. Hydrol. 349, 18–30. https://doi.org/10.1016/j.jhydrol.2007.10.055.

Bonnet, M.P., Pinel, S., Garnier, J., Bois, J., Resende Boaventura, G., Seyler, P., Motta Marques, D., 2017. Amazonian floodplain water balance based on modelling and analyses of hydrologic and electrical conductivity data. Hydrol. Process. 31, 1702–1718. https://doi.org/10.1002/hyp.11138.

Brunner, G.W., 2016. HEC-RAS river analysis system, User's Manual, Version 5.0. US Army Corps Eng. Hydrol. Eng. Center, Davis CA 960.

Callède, J., Cochonneau, G., Alves, F.V., Guyot, J.-L., Guimarães, V.S., De Oliveira, E., 2010. The River Amazon water contribution to the Atlantic Ocean. Rev. des Sci. l'eau 23, 247–273.

Cao, N., Lee, H., Jung, H.C., Yu, H., 2018. Estimation of Water Level Changes of Large-Scale Amazon Wetlands Using ALOS2 ScanSAR Differential Interferometry 10. 10.3390/rs10060966.

Chevuturi, A., Klingaman, N.P., Rudorff, C.M., Coelho, C.A.S., Schöngart, J., 2022. Forecasting annual maximum water level for the Negro River at Manaus. Clim. Resil. Sustain. 1, 1–17. https://doi.org/10.1002/cli2.18.

Chow, V. Te, 1959. Open-channel hydraulics. McGraw-Hill B. Co. 728. ISBN 07-010776-9.

Coe, M.T., Costa, M.H., Howard, E.A., 2008. Simulating the surface waters of the Amazon River basin: Impacts of new river geomorphic and flow parameterizations. Hydrol. Process. 22, 2542–2553. https://doi.org/10.1002/hyp.6850.

Collischonn, W., Allasia, D., da Silva, B.C., Tucci, C.E.M., 2007. The MGB-IPH model for large-scale rainfall-runoff modelling. Hydrol. Sci. J. 52, 878–895. https://doi.org/10.1623/hysj.52.5.878.

Correa, S.W., de Paiva, R.C.D., Espinoza, J.C., Collischonn, W., 2017. Multi-decadal Hydrological Retrospective: Case study of Amazon floods and droughts. J. Hydrol. 549, 667–684. https://doi.org/10.1016/j.jhydrol.2017.04.019.

de Paiva, R.C.D., Buarque, D.C., Collischonn, W., Bonnet, M.P., Frappart, F., Calmant, S., Bulhões Mendes, C.A., 2013. Large-scale hydrologic and hydrodynamic modeling of the Amazon River basin. Water Resour. Res. 49, 1226–1243. https://doi.org/10.1002/wrcr.20067.

Dunne, T., Mertes, L.A.K., Meade, R.H., Richey, J.E., Forsberg, B.R., 1998. Exchanges of sediment between the flood plain and chennel of the Amazon River in Brazil. Geol. Soc. Am. Bull. 110, 450–467. https://doi.org/10.1130/0016-7606(1998)110<0450.

Duponchelle, F., Isaac, V.J., Da Costa, R., Doria, C., Van Damme, P.A., Herrera-R, G.A., Anderson, E.P., Cruz, R.E.A., Hauser, M., Hermann, T.W., Agudelo, E., Bonilla-Castillo, C., Barthem, R., Freitas, C.E.C., García-Dávila, C., García-Vasquez, A., Renno, J.F., Castello, L., 2021. Conservation of migratory fishes in the Amazon basin. Aquat. Conserv. Mar. Freshw. Ecosyst. 31, 1087–1105. https://doi.org/10.1002/aqc.3550.

Fassoni-Andrade, A.C., Fleischmann, A.S., Paiva, R.C.D., 2020b. Lake topography and active storage from satellite observations of flood frequency. Water Resources Research 56 (7). https://doi.org/10.1029/2019wr026362.

Fassoni-Andrade, A.C., Fleischmann, A.S., Papa, F., de Paiva, R.C.D., Wongchuig, S., Melack, J.M., Moreira, A.A., Paris, A., Ruhoff, A., Barbosa, C., Maciel, D.A., Novo, E., Durand, F., Frappart, F., Aires, F., Abrahão, G.M., Ferreira-Ferreira, J., Espinoza, J. C., Laipelt, L., Costa, M.H., Espinoza-Villar, R., Calmant, S., Pellet, V., 2021. Amazon Hydrology From Space: Scientific Advances and Future Challenges. Rev. Geophys. 59, 1–97. https://doi.org/10.1029/2020RG000728.

Ferreira-Ferreira, J., Silva, T.S.F., Streher, A.S., Affonso, A.G., De Almeida Furtado, L.F., Forsberg, B.R., Valsecchi, J., Queiroz, H.L., De Moraes Novo, E.M.L., 2014. Combining ALOS/PALSAR derived vegetation structure and inundation patterns to characterize major vegetation types in the Mamirauá Sustainable Development Reserve, Central Amazon floodplain. Brazil. Wetl. Ecol. Manag. 23, 41–59. https://doi.org/10.1007/s11273-014-9359-1.

Filizola, N., Latrubesse, E.M., Fraizy, P., Souza, R., Guimarães, V., Guyot, J.L., 2014. Was the 2009 flood the most hazardous or the largest ever recorded in the Amazon? Geomorphology 215, 99–105. https://doi.org/10.1016/j.geomorph.2013.05.028.

Fleischmann, A.S., Paiva, R.C.D., Collischonn, W., Sorribas, M.V., Pontes, P.R.M., 2016. On river-floodplain interaction and hydrograph skewness. Water Resour. Res. 52, 7615–7630. https://doi.org/10.1002/2016WR019233.

Fleischmann, A.S., Paiva, R., Collischonn, W., 2019. Can regional to continental river hydrodynamic models be locally relevant? A cross-scale comparison. J. Hydrol. X 3, 100027. https://doi.org/10.1016/j.hydroa.2019.100027.

Fleischmann, A.S., Papa, F., Fassoni-Andrade, A., Melack, J.M., Wongchuig, S., de Paiva, R.C.D., Hamilton, S.K., Fluet-Chouinard, E., Barbedo, R., Aires, F., Al Bitar, A., Bonnet, M.-P., Coe, M., Ferreira-Ferreira, J., Hess, L., Jensen, K., Mcdonald, K., Ovando, A., Park, E., Parrens, M., Pinel, S., Prigent, C., Resende, A.F., Revel, M., Rosenqvist, A., Rosenqvist, J., Rudorff, C., Silva, T.S.F., Yamazaki, D., Collischonn, W., 2022. How much inundation occurs in the Amazon River basin? Remote Sens. Environ. 278, 67. https://doi.org/10.1002/essoar.10508718.1.

Frappart, F., Papa, F., Güntner, A., Tomasella, J., Pfeffer, J., Ramillien, G., Emilio, T., Schietti, J., Seoane, L., da Silva Carvalho, J., Medeiros Moreira, D., Bonnet, M.P., Seyler, F., 2019. The spatio-temporal variability of groundwater storage in the Amazon River Basin. Adv. Water Resour. 124, 41–52. https://doi.org/10.1016/j.advwatres.2018.12.005.

Fricke, A.T., Nittrouer, C.A., Ogston, A.S., Nowacki, D.J., Asp, N.E., Souza Filho, P.W.M., 2019. Morphology and dynamics of the intertidal floodplain along the Amazon tidal river. Earth Surf. Process. Landforms 44, 204–218. https://doi.org/10.1002/esp.4545.

Getirana, A.C.V., Boone, A., Yamazaki, D., Decharme, B., Papa, F., Mognard, N., 2012. The Hydrological Modeling and Analysis Platform (HyMAP): Evaluation in the Amazon Basin. J. Hydrometeorol. 13, 1641–1665. https://doi.org/10.1175/JHM-D-12-021.1.

Hess, L., Melack, J.M., Novo, E.M.L., Barbosa, C.F., Gastil, M., 2003. Dual-season mapping of wetland inundation and vegetation for the central Amazon basin. Remote Sens. Environ. 87, 404–428. https://doi.org/10.1016/j.rse.2003.04.001.

Hess, L.L., Melack, J.M., Affonso, A.G., Barbosa, C., Gastil-Buhl, M., Novo, E.M.L.M., 2015. Wetlands of the Lowland Amazon Basin: Extent, Vegetative Cover, and Dual-season Inundated Area as Mapped with JERS-1 Synthetic Aperture Radar. Wetlands 35, 745–756. https://doi.org/10.1007/s13157-015-0666-y.

Jahfer, S., Vinayachandran, P.N., Nanjundiah, R.S., 2017. Long-Term impact of Amazon river runoff on northern hemispheric climate. Sci. Rep. 7, 1–9. https://doi.org/10.1038/s41598-017-10750-y.

Ji, X., Lesack, L.F.W., Melack, J.M., Wang, S., Riley, W.J., Shen, C., 2019. Seasonal and inter-annual patterns and controls of hydrological fluxes in an Amazon floodplain lake with a surface-subsurface processes model. Water Resour. Res. 55, 3056–3075. https://doi.org/10.1029/2018WR023897.

Latrubesse, E.M., Franzinelli, E., 2002. The Holocene alluvial plain of the middle Amazon River, Brazil. Geomorphology 44, 241–257. https://doi.org/10.1016/S0169-555X(01)00177-5.

LeFavour, G., Alsdorf, D., 2005. Water slope and discharge in the Amazon River estimated using the shuttle radar topography mission digital elevation model. Geophys. Res. Lett. 32, 1–5. https://doi.org/10.1029/2005GL023836.

Lesack, F.W., Melack, J.M., 1995. Flooding hydrology and mixture dynamics of lakewater derived from multiple sources in an Amazon floodplain lake. Water Resour. Res. 31, 329–345.

Luo, X., Li, H.Y., Ruby Leung, L., Tesfa, T.K., Getirana, A., Papa, F., Hess, L.L., 2017. Modeling surface water dynamics in the Amazon Basin using MOSART-Inundation v1.0: Impacts of geomorphological parameters and river flow representation. Geosci. Model Dev. 10, 1233–1259. https://doi.org/10.5194/gmd-10-1233-2017.

Meade, R.H., Rayol, J.M., Da Conceicão, S.C., Natividade, J.R.G., 1991. Backwater effects in the Amazon River basin of Brazil. Environ. Geol. Water Sci. 18, 105–114. https://doi.org/10.1007/BF01704664.

Melack, J.M., Novo, E.M.L.M., Forsberg, B.R., Piedade, M.T.F.F., Maurice, L., 2009. Floodplain Ecosystem Processes. Amaz. Glob. Chang. 525–541 https://doi.org/10.1029/2008GM000727.

Fassoni-Andrade, A.C., Paiva, R.C.D., Rudorff, C.M., Barbosa, C.C.F., de M. Novo, E.M.L., 2020a. High-resolution mapping of floodplain topography from space: A case study in the Amazon. Remote Sens. Environ. 251, 112065 https://doi.org/10.1016/j.rse.2020.112065.

Moreira, A.A., Ruhoff, A.L., Roberti, D.R., Souza, V. de A., da Rocha, H.R., de Paiva, R.C. D., 2019. Assessment of terrestrial water balance using remote sensing data in South America. J. Hydrol. 575, 131–147. 10.1016/j.jhydrol.2019.05.021.

Nash, J.E., Sutcliffe, J.V., 1970. River Flow Forecasting Through Conceptual Models Part I-a Discussion of Principles*. J. Hydrol. 10, 282–290. https://doi.org/10.1016/0022-1694(70)90255-6.

Papa, F., Frappart, F., Güntner, A., Prigent, C., Aires, F., Getirana, A.C.V., Maurer, R., 2013. Surface freshwater storage and variability in the Amazon basin from multi-satellite observations, 1993–2007. J. Geophys. Res. Atmos. 118, 11951–11965. https://doi.org/10.1002/2013JD020500.

Pinel, S., Bonnet, M.-P., Santos Da Silva, J., Moreira, D., Calmant, S., Satgé, F., Seyler, F., 2015. Correction of Interferometric and Vegetation Biases in the SRTMGL1 Spaceborne DEM with Hydrological Conditioning towards Improved Hydrodynamics Modeling in the Amazon Basin. Remote Sens. 7, 16108–16130. https://doi.org/10.3390/rs71215822.

Pinel, S., Bonnet, M., Silva, J.S. Da, Sampaio, T.C., Garnier, J., Catry, T., Calmant, S., Jr, C.R.F., Moreira, D., Marques, D.M., Seyler, F., 2019. Flooding dynamics within a Amazonian floodplain : Water circulation patterns and inundation duration. Water Resour. Res. 56. 10.1029/2019WR026081.

Pugh, D., Woodworth, P., 2014. Sea-Level Science: Understanding Tides, Surges, Tsunamis and Mean Sea-Level Changes. Oceanography. https://doi.org/10.5670/oceanog.2015.24.

Richey, J.E., Mertes, L.K., Dunne, T., Victoria, R.L., Forsberg, B.R., Tancredi, A.C.N.S., de Oliveira, E., 1989. Sources and routing of the Amazon River flood wave 3, 191–204.

Richey, J.E., Spencer, R.G.M., Drake, T.W., Ward, N.D., 2022. Fluvial Carbon Dynamics across the Land to Ocean Continuum of Great Tropical Rivers. In: Congo Basin Hydrology, Climate, and Biogeochemistry. American Geophysical Union (AGU), pp. 391–412. https://doi.org/10.1002/9781119657002.ch20.

Rosenqvist, J., Rosenqvist, A., Jensen, K., McDonald, K., 2020. Mapping of maximum and minimum inundation extents in the amazon basin 2014–2017 with ALOS-2 PALSAR-2 scan SAR time-series data. Remote Sens. 12 https://doi.org/10.3390/RS12081326.

Rudorff, C.M., Melack, J.M., Bates, P.D., 2014a. Flooding dynamics on the lower Amazon floodplain: 1. Hydraulic controls on water elevation, inundation extent, and river-floodplain discharge. Water Resour. Res. 50, 619–634. https://doi.org/10.1002/2013WR014091.

Rudorff, C.M., Melack, J.M., Bates, P.D., 2014b. Flooding dynamics on the lower Amazon floodplain: 2. Seasonal and interannual hydrological variability. Water Resour. Res. 50, 635–649. https://doi.org/10.1002/2013WR014714.

Schumann, G., Bates, P.D., Horritt, M.S., Matgen, P., Pappenberger, F., 2009. Progress in Integration of Remote Sensing-Derived Flood Extent and Stage Data and Hydraulic Models. Rev. Geophys. 47, 1–20. https://doi.org/10.1029/2008rg000274.

Silva, J.S.D., Calmant, S., Seyler, F., Rotunno Filho, O.C., Cochonneau, G., Mansur, W.J., 2010. Water levels in the Amazon basin derived from the ERS 2 and ENVISAT radar altimetry missions. Remote Sens. Environ. 114, 2160–2181. https://doi.org/10.1016/j.rse.2010.04.020.

Siqueira, V.A., Paiva, R.C.D., Fleischmann, A.S., Fan, F.M., Ruhoff, A.L., Pontes, P.R.M., Paris, A., Calmant, S., Collischonn, W., 2018. Toward continental hydrologic-hydrodynamic modeling in South America. Hydrol. Earth Syst. Sci. 22, 4815–4842. https://doi.org/10.5194/hess-22-4815-2018.

Sorribas, M.V., de Paiva, R.C.D., Fleischmann, A.S., Collischonn, W., 2020. Hydrological Tracking Model for Amazon Surface Waters. Water Resour. Res. 56, 1–19. https://doi.org/10.1029/2019WR024721.

Trigg, M.A., Wilson, M.D., Bates, P.D., Horritt, M.S., Alsdorf, D.E., Forsberg, B.R., Vega, M.C., 2009. Amazon flood wave hydraulics. J. Hydrol. 374, 92–105. https://doi.org/10.1016/j.jhydrol.2009.06.004.

Trigg, M.A., Bates, P.D., Wilson, M.D., Schumann, G., Baugh, C., 2012. Floodplain channel morphology and networks of the middle Amazon River. Water Resour. Res. 48, 1–17. https://doi.org/10.1029/2012WR011888.

Tull, N., Passalacqua, P., Hassenruck-Gudipati, H.J., Rahman, S., Wright, K., Hariharan, J., Mohrig, D., 2022. Floodplain Connectivity During Combined Pluvial-Fluvial Events. Water Resour. Res. 58, 1–24. https://doi.org/10.1029/2021WR030492.

Wilson, M.D., Bates, P., Alsdorf, D., Forsberg, B., Horritt, M., Melack, J., Frappart, F., Famiglietti, J., 2007. Modeling large-scale inundation of Amazonian seasonally flooded wetlands. Geophys. Res. Lett. 34, 4–9. https://doi.org/10.1029/2007GL030156.

Wohl, E., 2021. An Integrative Conceptualization of Floodplain Storage. Rev. Geophys. 59, 1–63. https://doi.org/10.1029/2020RG000724.

Yamazaki, D., Kanae, S., Kim, H., Oki, T., 2011. A physically based description of floodplain inundation dynamics in a global river routing model. Water Resour. Res. 47 https://doi.org/10.1029/2010WR009726.

Yamazaki, D., Baugh, C.A., Bates, P.D., Kanae, S., Alsdorf, D.E., Oki, T., 2012a. Adjustment of a spaceborne DEM for use in floodplain hydrodynamic modeling. J. Hydrol. 436–437, 81–91. https://doi.org/10.1016/j.jhydrol.2012.02.045.

Yamazaki, D., Lee, H., Alsdorf, D.E., Dutra, E., Kim, H., Kanae, S., Oki, T., 2012b. Analysis of the water level dynamics simulated by a global river model: A case study in the Amazon River. Water Resour. Res. 48, 1–15. https://doi.org/10.1029/2012WR011869.

Yamazaki, D., Ikeshima, D., Tawatari, R., Yamaguchi, T., O'Loughlin, F., Neal, J.C., Sampson, C.C., Kanae, S., Bates, P.D., 2017. A high-accuracy map of global terrain elevations. Geophys. Res. Lett. 44, 5844–5853. https://doi.org/10.1002/2017GL072874.

Zhang, Q., Werner, A.D., 2015. Hysteretic relationships in inundation dynamics for a large lake-floodplain system. J. Hydrol. 527, 160–171. https://doi.org/10.1016/j.jhydrol.2015.04.068.